

LEVEL 4

6

5

AD A101088

FINAL TECHNICAL REPORT

to the

AIR FORCE OFFICE OF SCIENTIFIC RESEARCH

from

Eugene Herrin

and

Tom Goforth

Geophysical Laboratory
Southern Methodist University
Dallas, Texas 75275

DTIC
ELECTE
JUL 7 1981

A

ARPA Order: 3291

Program Code: 7F10

Name of Contractor: Southern Methodist University

Effective Date of Contract: 15 July 1976

Contract Expiration Date: 31 October 1980

Total Amount of Contract: \$579,294

Contract Number: F49620-76-C-0030

Principal Investigators and Phone Number: Eugene Herrin

Tom Goforth

AC 214 692-2760

Program Manager and Phone Number: Truman Cook, Director of
Research Administration

AC 214 692-2031

Title of Work: Propagation Path Effects for Rayleigh and
Love Waves

University Account Number: 5-25019

Sponsored by
Defense Advanced Research Projects Agency

Approved for public release;
distribution unlimited.

01 00 021

DTIC FILE COPY

19 REPORT DOCUMENTATION PAGE		READ INSTRUCTIONS BEFORE COMPLETING FORM	
1. REPORT NUMBER AFOSR/TR-81-0534	2. GOVT ACCESSION NO. AD-A101088	3. RECIPIENT'S CATALOG NUMBER (9)	
4. TITLE (and Subtitle) PROPAGATION PATH EFFECTS FOR RAYLEIGH AND LOVE WAVES.		5. TYPE OF REPORT & PERIOD COVERED Scientific Final rept. 15 Jul 76 - 31 Oct 80	
6. AUTHOR(s) Eugene Herrin Tom Goforth		7. CONTRACT OR GRANT NUMBER(s) F49620-76-C-0030 ARPA order-3891	
8. PERFORMING ORGANIZATION NAME AND ADDRESS Geophysical Laboratory Southern Methodist University Dallas, TX 75275		9. PROGRAM ELEMENT, PROJECT, TASK AREA & WORK UNIT NUMBERS 3291 7E10 62701E	
10. CONTROLLING OFFICE NAME AND ADDRESS ARPA/NMR 1400 Wilson Blvd. Arlington, VA 22209		11. REPORT DATE May 1981	
12. MONITORING AGENCY NAME & ADDRESS (if different from Controlling Office) AFOSR/NP Bolling AFB Wash DC 20332		13. NUMBER OF PAGES 92	
14. DISTRIBUTION STATEMENT (of this Report) Approved for public release; distribution unlimited.		15. SECURITY CLASS. (of this report) unclassified	
16. DISTRIBUTION STATEMENT (of the abstract entered in Block 20, if different from Report)		15a. DECLASSIFICATION/DOWNGRADING SCHEDULE	
17. SUPPLEMENTARY NOTES			
18. KEY WORDS (Continue on reverse side if necessary and identify by block number)			
19. ABSTRACT (Continue on reverse side if necessary and identify by block number) Phase-matched filters have been developed for several paths of interest for both Rayleigh and Love waves. The filters are presented in the form of tabled values of apparent group velocity as a function of frequency. Detailed instructions are given as to how the tabled values can be used to construct phase-matched filters and how the filters can be applied to low-level signals which have travelled the same path. Application of the filters provides a time series in which the effects of multipaths have been minimized and on which the signal-to-noise ratio			

is improved by a factor proportional to the time compression of the signal achieved by the filtering. For a signal bandwidth of 0.1 - 0.015 Hz and an epicentral distance of 30 degrees, the signal-to-noise ratio is about 10 dB better than on the original seismogram. The filtered seismogram can be used for the determination of surface wave magnitude.

UNCLASSIFIED

SECURITY CLASSIFICATION OF THIS PAGE (When Data Entered)

ABSTRACT

This report presents the results of all the studies which were completed during the period 15 July 1976 through 31 October 1980 under AFOSR Contract F49620-76-C-0030. Many of these studies have been submitted previously to AFOSR in the form of Technical Reports, and the results of these studies are covered here only in summary and abstract form. Complete reports are presented, however, for a study of the crustal structure of Yucca Flat and for the establishment of a new seismic station in the Big Bend area of southwest Texas.

Accession For	
NTIS GRA&I	<input checked="checked" type="checkbox"/>
DTIC TAB	<input type="checkbox"/>
Unannounced	<input type="checkbox"/>
Justification	
By	
Distribution/	
Availability Codes	
Dist	Avail and/or Special
A	

AIR FORCE OFFICE OF SCIENTIFIC RESEARCH (AFSC)

NOTICE OF TRANSMITTAL TO DDC

This technical report has been reviewed and is approved for public release IAW AFR 190-12 (7b). Distribution is unlimited.

A. D. ROSE

Technical Information Officer

INTRODUCITON

During the period 15 July 1976 to 31 October 1980 a group of studies directed toward the improvement in techniques of detection and analysis of seismic body and surface waves were completed by the Geophysical Laboratory of Southern Methodist University. Many of these studies have been reported to AFOSR previously in the form of Technical Reports and as articles in the periodic scientific literature. Abstracts of the previously-published research efforts are included, and a brief summary of each of the studies follows.

A study in 1976 demonstrated that the effects of wind generated noise on long-period seismographs could be predicted from the atmospheric pressure changes recorded by a microbarograph located at the same site. It was found, however, that the efficiency of the prediction depends on the wind direction, wind speed, and the variance of the wind speed. The turbulent cells associated with atmospheric pressure changes are believed to be broken down into smaller cells as the speed and variability of the wind increase. The increase of high frequency energy contributed by smaller cell disturbances also increases the nonlinear part of the transfer function and hence breaks down the prediction ability of the linear filter (Technical Report to AFOSR, March 1977).

Phase-matched filters were developed for several paths of interest for both Rayleigh and Love waves. Application of the filters to low-level signals which have travelled the same path

provides a time series in which the effects of multipaths have been minimized and in which the signal-to-noise ratio is improved by a factor proportional to the time compression of the signal achieved by the filtering (Technical Report to AFOSR, February, 1978; Bull. Seis. Soc. Am., October, 1977; Bull. Seis. Soc. Am., February, 1979) .

A theoretical study was completed which describes the effects on the attenuation and phase velocity of Raleigh waves propagating across a vertical boundary separating two layered, viscoelastic media (Technical Report to AFOSR, July, 1979; Bull. Seis. Soc. Am., submitted 1980).

The velocity structures of the Bering Sea and southern Alaska areas were determined by applying a generalized linear inversion method to fundamental-mode Rayleigh wave group velocity curves obtained from phase-matched filtering of digitally recorded data. A new exact analytical method for the computation of Rayleigh wave phase velocity partial derivatives with respect to earth parameters was formulated (Technical Report to AFOSR, January, 1979; Bull. Seis. Soc. Sm., December, 1980).

An automatic seismic signal algorithm based on the Walsh transform was developed. The Walsh transform can be accomplished in a computer with a series of shifts and fixed point additions such that the savings in computation time makes it possible to compute the transform and to perform pre-whitening and bandpass filtering in real time on a hobby-class microprocessor for use in signal detection. Tests utilizing seismic data recorded in Dallas, Albuquerque, and Norway indicate that the algorithm has

a detection capability compared to that of an experienced human analyst (Technical Report ot AFOSR, January, 1980; Bull. Seis. Soc. Am., in publication).

During 1978 a seismic reflection survey was conducted at Yucca Flat on the Nevada Test Site. A total of 25 line miles was surveyed, including two east-west profiles perpendicular to the trend of the valley and one north-south profile parallel to the trend. Two-dimensional interpretation of the profiles revealed a fault not previously mentioned in the literature. The fault was shown to be significantly larger in throw than the well-known Yucca fault (Technical Report to AFOSR, July, 1979; EOS abstract, December, 1980). Using the seismic data, a three-dimensional model which is consistent with gravity and borehole data has been constructed for Yucca Flat. The present report fully documents the development of the three-dimensional model.

In the last few months a new seismic station has been established near Lajitas, Texas. That protion of southwest Texas within the Big Bend of the Rio Grande is ideally situated to monitor siesmic events at both regional and teleseismic distances. Two 350-foot holes were drilled according to specifications suitable for the installation of Geotech KS-36000 seismometer. A 120-foot hole was also drilled, and it presently contains an operational Geotech 23900 vertical seismometer. Data from the short-period 23900 along with broad-band data from the Albuquerque Seismic Research Observatory (SRO) and the McKinney, Texas, KS-36000 site are currently being transmitted to the SMU Geophysical Laboratory via telephone lines. The imminent installation of a

KS-36000 at Lajitas will complete the broad-band, tripartite network. On-line, automatic detection of short-period signals will be accomplished by a microprocessor in the SMU laboratory. Both short-period and long-period network data will be available for off-line processing, including epicenter and magnitude (M_b and M_s) determinations. A complete description of the Lajitas site is included in this report.

PREDICTION AND ELIMINATION OF PRESSURE
GENERATED GROUND NOISE ON LONG PERIOD
SEISMOGRAMS USING OPTIMUM FILTERS

Jennifer Young, Eugene Herrin,
and Tom Goforth
Geophysical Laboratory
Southern Methodist University
March 1977

ABSTRACT

Seismic noise generated by surface winds severely limits the usefulness of long-period seismograms. A linear dependence is observed between the recordings of a long-period seismograph and a co-located microbarograph in the period range 20 to 100 seconds. It is possible to design a filter, based on the least-mean-square method, such that the effects of the wind generated noise on the seismograph may be predicted from the atmospheric pressure changes recorded by a microbarograph located at the same site. The filter has been used to reduce the noise level for seismic data and hence increase the S/N ratio. However, only limited success has been achieved, and the efficiency of the prediction tends to depend on the wind direction, wind speed and the variance of the wind speed. The turbulent cells associated with atmospheric pressure changes are believed to be broken down into smaller cells as the speed and variability of the wind increase. The increase of high frequency energy contributed by smaller cell disturbances also increases the nonlinear part of the transfer function and hence breaks down the prediction ability of the filter.

CRUSTAL STUDIES OF THE NEVADA TEST SITE:
INTERPRETATION OF SMU LINE E-3

by

Tom Goforth, John Ferguson
and
Eugene Herrin

Geophysical Laboratory
Institute for the Study of Earth and Man
Southern Methodist University
July 1979

CRUSTAL STUDIES OF THE NEVADA TEST SITE

ABSTRACT

During January 1978 a seismic reflection survey was conducted at Yucca Flat on the Nevada Test Site. A total of 25 line miles was surveyed, including two east-west profiles perpendicular to the trend of the valley and one north-south profile parallel to the trend. Four Y-900 LF vibrators were used to generate signals. Because of the expected high attenuative characteristics of the dry alluvium in Yucca Flat, 4.5 Hz geophones and low-frequency sweeps were employed. A structural cross-section which is consistent with gravity and borehole data is presented for the southern portion of Yucca Flat.

PHASE-MATCHED FILTERS FOR
SELECTED SOURCE-RECEIVER PATHS

by

Tom Goforth

Geophysical Laboratory
Southern Methodist University
Dallas, Texas 75275
28 February 1978

ABSTRACT

Phase-matched filters have been developed for several paths of interest for both Rayleigh and Love waves. The filters are presented in the form of tabled values of apparent group velocity as a function of frequency. Detailed instructions are given as to how the tabled values can be used to construct phase-matched filters and how the filters can be applied to low-level signals which have travelled the same path. Application of the filters provides a time series in which the effects of multipaths have been minimized and on which the signal-to-noise ratio is improved by a factor proportional to the time compression of the signal achieved by the filtering. For a signal bandwidth of 0.1 - 0.015 Hz and an epicentral distance of 30 degrees, the signal-to-noise ratio is about 10 dB better than on the original seismogram. The filtered seismogram can be used for the determination of surface wave magnitude.

SURFACE WAVE STUDIES
OF THE
BERING SEA AND ALASKA AREA

by
Doo Jung Jin

Geophysical Laboratory
Southern Methodist University
Dallas, Texas 75275
31 January 1979

ABSTRACT

The area of the Bering Sea and Alaska has been studied in terms of shear-velocity, density and compressional-velocity structure by applying a generalized linear inversion method to fundamental-mode Rayleigh-wave group-velocity dispersion relationships in the period range from 10 to 100 sec.

Group velocity dispersion relationships in the area have been obtained by applying the phase-matched filtering technique (Herrin and Goforth, 1977) to digitally recorded surface-wave data. Corrections for instrument response and the sphericity of the Earth were applied to the dispersion observations. A new exact analytical method for the computation of Rayleigh-wave phase-velocity partial derivatives with respect to Earth parameters has been formulated. With the phase-velocity partial derivatives determined, the group velocity partial derivatives were computed by use of the fast and accurate method of Rodi et al. (1975), and were successfully incorporated into a generalized linear inversion method.

The study area has been found to consist of three physiographic provinces and the structure of the three regions has been estimated as follows: In continental Alaska, the crustal thickness is 43 ± 3 km, and a low velocity zone extends from a depth of about 113 km to about 213 km. In the Bering Shelf region, the depth to the Mohorovicic discontinuity is 28 ± 4 km, and a low velocity zone ranges in depth from about 108 km to about 213 km. In the Aleutian Basin, the thickness of the crust is 18 ± 4 km, and a low velocity zone extends from a depth of about 60 km to about 220 km.

ENERGY DISSIPATION OF RAYLEIGH WAVES DUE TO ABSORPTION
ALONG THE PATH BY THE USE OF FINITE ELEMENT METHOD

by

Ali A. Feizpour

Geophysical Laboratory
Southern Methodist University
Dallas, Texas 75275
31 July 1979

ABSTRACT

A normally incident Rayleigh wave may be used for the investigation of a general vertical boundary and the attenuation of a viscoelastic medium. Use of energy conservation and proper boundary conditions produce $2N$ second order differential equations, N being the number of viscoelastic layers in the medium. The homogeneous part of the differential equations can be transformed into an eigenvalue problem by the use of finite element technique; the eigenvalue and eigenvectors of the eigenvalue problem are the wavenumbers and the displacement amplitudes of the viscoelastic layered medium. The real and imaginary parts of the wavenumber determine the phase velocity and the attenuation of the layered medium, respectively. Dispersion and the attenuation curves can be obtained by using different periods. The above wavenumbers can be used in the inhomogeneous differential equation; this equation contains the effect of the vertical boundary; solution of this equation determines the displacement at the vertical boundary. The displacements at the left and right sides of the boundary may be used in the energy equation to determine the reflected and the transmitted energy, respectively. The difference between

the incident and transmitted energy determines the difference between the wavenumbers at the left and right hand sides of the vertical boundary. Addition of these differences to the wavenumbers of the left hand boundary would result in the formation of the dispersion curve at the right hand boundary.

PHASE-MATCHED FILTERS: APPLICATION TO
THE STUDY OF LOVE WAVES

by Tom Goforth and Eugene Herrin

Geophysical Laboratory
Southern Methodist University
Dallas, Texas 75275
April 1978

ABSTRACT

Seismic surface waves are usually composed of overlapping wave trains representing multi-path propagation. A first task in the analysis of such waves is to identify and separate the various component wave trains so that each can be analyzed separately.

Phase-matched filters are a class of linear filters in which the Fourier phase of the filter is made equal to that of a given signal. Herrin and Goforth (1977) described an iterative technique which can be used to find a phase-matched filter for a particular component of a seismic signal. Application of the filters to digital records of Rayleigh waves allowed multiple arrivals to be identified and removed, and allowed recovery of the complex spectrum of the primary wave train along with its apparent group velocity dispersion curve.

A comparable analysis of Love waves presents additional complications. Love waves are contaminated by both Love and Rayleigh multipathing and by primary off-axis Rayleigh energy. In the case of explosions, there is much less energy generated as Love waves than as Rayleigh waves.

The applicability of phase-matched filtering to Love waves is demonstrated by its use on earthquakes occurring in

the Norwegian Sea and near Iceland and on a nuclear explosion in Novaya Zemlya. Despite severe multipathing in two of the three events, the amplitude and phase of each of the primary Love waves were recovered without significant distortion.

AN AUTOMATIC SEISMIC SIGNAL DETECTION
ALGORITHM BASED ON THE WALSH TRANSFORM

by

Tom Goforth

and

Eugene Herrin

Geophysical Laboratory
Southern Methodist University
Dallas, Texas 75275
March 10, 1980

ABSTRACT

An automatic seismic signal detection algorithm based on the Walsh transform has been developed. Since the amplitude of a Walsh function is either +1 or -1, the Walsh transform can be accomplished in a computer with a series of shifts and fixed point additions. The savings in computation time makes it possible to compute the Walsh transform and to perform band-pass, pre-whitening and adaptive filtering with a micro-computer in real time for use in signal detection.

The algorithm has been programmed in FORTRAN on a Raytheon Data Systems 500 mini-computer. Tests utilizing seismic data recorded in Dallas, Albuquerque, and Norway indicate that the algorithm has a detection capability comparable to a human analyst. The Walsh detection algorithm runs in approximately 1/10 real time on the RDS-500 mini-computer. Programming of the detection system in machine language on a North Star Horizon microprocessor-based computer is almost complete. Run time on the Horizon is estimated to be 1/3 real time.

LAJITAS SEISMIC STATION
Site Report

LAJITAS SEISMIC STATION
Site Report

Introduction

A number of unpublished seismic noise studies during the last 20 Years, mostly by E. Herrin, W. Guyton, J. Waugh and B. Brooks, have shown that sites in the limestone desert region just west of Big Bend National Park, Brewster County, Texas, show very low short-period noise levels. Peak-to-peak displacements at the surface in the absence of wind or other obvious disturbances have amplitudes less than 10^{-9} meter at a frequency of 1 Hz. and less than 10^{-10} meter at 10 Hz.

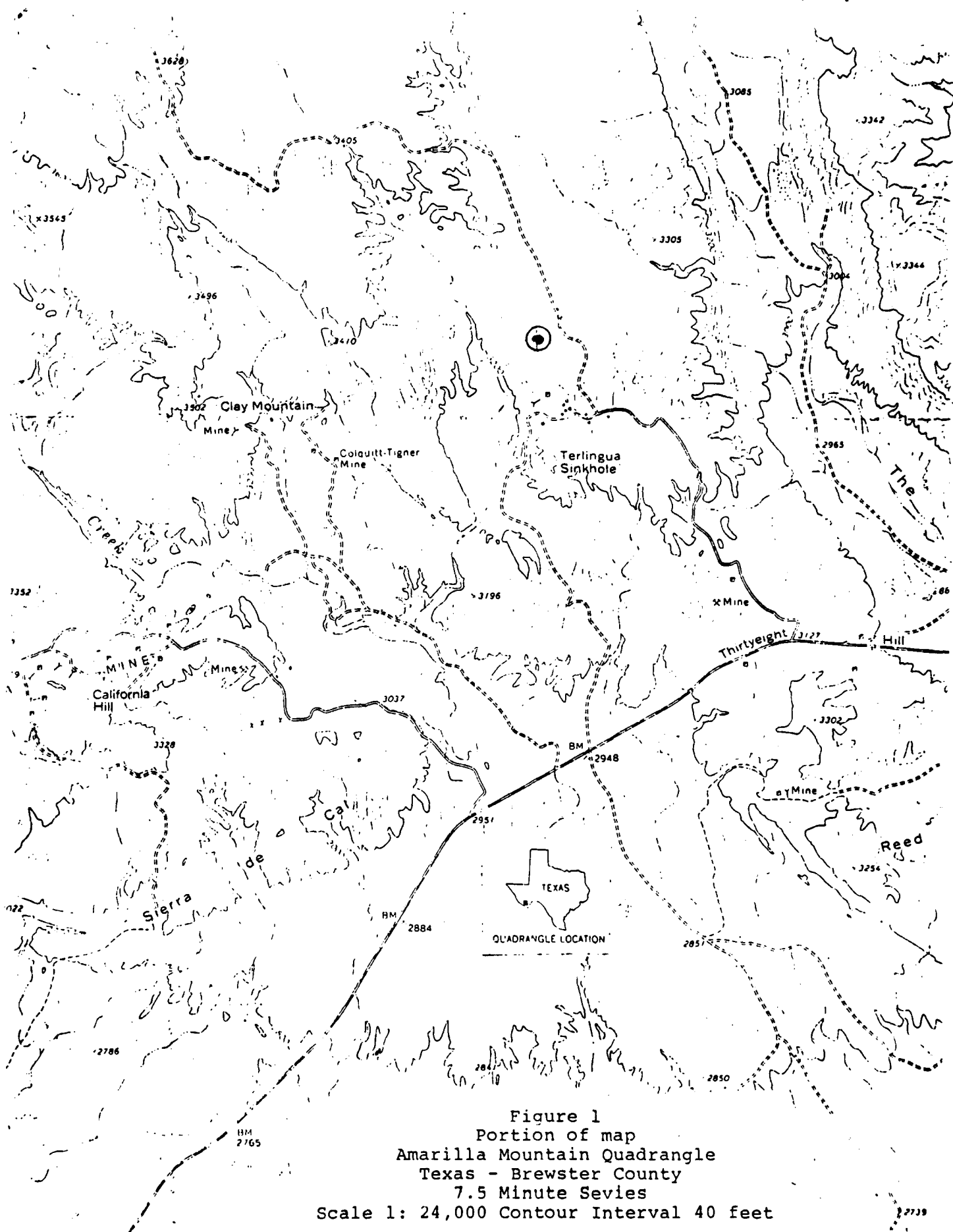
The area studied is very sparsely settled and has only one paved highway which is lightly travelled. The nearest railroad is 40 miles to the west and has only a few trains per week. The nearest heavily travelled highway and railroad, and the nearest town of any size - Alpine, Texas - is about 75 miles to the north of the area. We have obtained a lease on private land in this area and have established the Lajitas Seismic Station which is described in this report.

Location

The Lajitas Station is located about 10 miles by road northeast of Lajitas, Texas, a small village on the Rio Grande just west of Big Bend National Park. The site location is shown as a circled dot just north of Terlingua Sinkhole on Figure 1, and is on land owned by Mr. Glen Pepper. Pertinent information on the location is as follows:

Coordinates: 29° 20.0' North latitude
 103° 40.0' West longitude
Elevation: 3325 feet above mean sea level

The paved road (Texas FM 170) and graded road to Pepper's hacienda about $\frac{1}{4}$ mile south-southeast of the site can be seen in Figure 1. These roads provide all-weather access to the site and to Lajitas, Texas, to the west and Study Butte, Texas, to the east. The remoteness of the site is important in that man-made noise is minimal but leads to certain logistical problems. For example, the nearest scheduled airline service is to be found at Midland, Texas, 250 miles to the northeast and El Paso, Texas, 300 miles to the northwest.



Geology

The Lajitas site lies on the top of the Santa Elena formation, a massive limestone unit of Cretaceous (Upper Albian) age. Cretaceous formations beneath the site are listed under the heading "Big Bend National Park Area" in the correlation table shown in Figure 2. Table 1 gives thicknesses and brief descriptions of the underlying Cretaceous formations as seen in exposures in Santa Elena Canyon (SEC) about 12 miles southeast and The Solitario (SOL) about 8 miles northwest of the site. The Santa Elena Canyon data are from Maxwell et. al., 1967, Univ. of Texas Publ. 6711, Bu. of Economic Geology, and The Solitario data are from Herrin, 1958, Geology of the Solitario area, Trans-Pecos Texas, Harvard University.




From Table 1 it can be seen that the site is underlain by more than 3600 feet of lower Cretaceous sediments consisting predominantly of massive limestones which should have P-wave velocities in excess of 5 km/sec.

The uppermost 800 ft consists of the massive, dense Santa Elena formation. Beneath the basal Cretaceous conglomerate (Shut Up formation) there are several thousand feet of folded Paleozoic sediments, mostly siliceous shales with some chert and limestone, underlain by a Cambrian and older basement complex.

The site is on a horst bounded on the east by a normal fault on the west side of the Long Draw graben and represented by the fault-line scarp seen on Figure 1 about $\frac{1}{2}$ mile east of

Table 1

<u>Formation</u>	Thickness (feet)		<u>Description</u>
	<u>SEC</u>	<u>SOL</u>	
Santa Elena	740	820	Massive hard limestone with bedded chert
Sue Peaks	265	187	Marly limestone - Thin to medium bedded
Del Carmen	465	685	Massive, hard, cherty rudistid limestone
Telephone Canyon	135	190	Nodular limestone and marl - thin to medium bedded
Maxon	0-10	0	Calcareous sandstone
Glen Rose	?	1154	Alternating units of massive limestone and highly fossiliferous marl
Yucca	?	482	Sandy limestone and dolomite grading into massive limestone at top
Shut Up	?	100	Chert boulder basal conglomerate

SYSTEM	EUROPEAN STAGES	REFERENCE SEQUENCE FOR WESTERN INTERIOR	SERIES	GROUP	BIG BEND NATIONAL PARK AREA	RIO GRANDE EMBAYMENT OF SOUTHWEST TEXAS (Surface and Subsurface)	CENTRAL TEXAS	NORTHEAST TEXAS (Surface and Subsurface)		
CRETACEOUS	MAESTRICHTIAN	Fox Hills Sand-stone	GULFIAN	TORNILLO	Javelina Formation Contains dinosaur bones, silicified wood, and coal beds	Escondido Formation	Kemp Clay	Kemp Clay		
						Olmec Formation	Corsicana Marl	Corsicana Marl		
						Upper San Miguel Formation		Nacatoch Sand-stone		
	CAMPANIAN	Pierre Shale			Continental sand-stone and shale with Upper Campanian age dinosaur bones	Lower San Miguel Formation	Bergstrom Formation	Neylandville Marl		
					Marine sand-stone and shale with <i>Exogyra ponderosa</i> and <i>Texanites</i> sp.	Anacacho Limestone	Pecan Gap Chalk and Clay	Pecan Gap Chalk		
								Wolfe City Sandstone		
						Upson Clay (with <i>Exogyra ponderosa</i> and <i>Texanites</i> sp.)	Sprinkle Formation	Lower Taylor Formation		
					Eagle Sand-stone				Gober Chalk	
					Telephone Creek Formation	Pen Formation (with <i>Exogyra ponderosa</i>)	Burditt Chalk	Burditt Chalk	Brown-town Marl	
						Austin Chalk (with <i>Exogyra ponderosa</i>)	Dessau Chalk (with <i>Exogyra ponderosa</i>)			
	SANTONIAN									
	CONIACIAN	Niobrara Formation		BOQUILLAS FORMATION	San Vicente Member (without <i>Exogyra ponderosa</i>)	Austin Chalk (without <i>Exogyra ponderosa</i>)	Jonah Limestone	Blossom Sand-stone		
							Vinson Chalk	Bonham Clay		
							Aten Chalk	Eaton Chalk		
	TURONIAN	Carlisle Shale		Ernst Member	Eagle Ford Formation	Eagle Ford Formation	Eagle Ford Formation			
							Lewisville Formation (volcanics)			
	CENOMANIAN	Greenhorn Limestone								
		Belle Fourche Formation				Pepper Formation	Eules Formation			
							Dexter Formation			
		Mowry Shale		Buda Limestone	Buda Limestone	Buda Limestone	South Tyler Formation			
	ALBIAN	Upper		Newcastle Sand-stone	Santa Elena Limestone	Georgetown Limestone (undifferentiated)	Georgetown Limestone (undifferentiated)	Main Street Limestone		
								Pawpaw Formation		
		Middle		Skull Creek Shale		Duck Creek Formation (ammonites near base)		Weno Formation		
						Kiamichi Formation	Kiamichi Formation	Denton Formation		
				Falls River Sand-tone	Del Carmen Limestone	Fredricksburg (undifferentiated)	Edwards Limestone	Fort Worth Limestone		
					Telephone Canyon Formation		Comanche Peak Limestone	Duck Creek Limestone		
					Walnut Clay	Kiamichi Formation				
			Mason Sand-tone			Paluxy Sand-tone	Paluxy Sandstone			
Lower		Red shale	Glen Rose Limestone (undifferentiated) with basal sandstone and conglomerate	Glen Rose Formation (undifferentiated)	Glen Rose Formation (undifferentiated)	GLEN ROSE FORMATION	Mooringsport Formation			
							Ferry Lake Anhydrite			
						Rodessa Formation				

the circled dot. The horst is bounded on the west by a series of normal faults, mostly down-thrown to the west, culminating in the Well Creek graben which lies just north of California Hill. It is possible that this arrangement of normal faults serves to shield the site from short wave-length surface waves propagating from noise sources which do not lie on the horst.

Drilling Operations

Dick Baker Drilling Company of Marfa, Texas, began operations at the site on 8 Sept. 1980. Operations, including drilling, setting casing and cementing three holes, were completed on 19 Sept. 1980. The three holes are located with ten-foot spacing on a north-northeast bearing line-of-centers. The north-most hole is labelled number 1; the south-most is number three. Specifications for the holes are given in Table 2.

Table 2

<u>Hole</u>	<u>(inches) Diameter</u>	<u>(feet) Total Depth</u>	<u>Maximum Inclination</u>
1	9 7/8	352	2° (at 350 ft)
2	7 7/8	122	1° (at 120 ft)
3	9 7/8	350	1½° (at 350 ft)

Holes number 1 and 3 were cased and cemented to the bottom with API 7" OD 23# casing. Hole number 2 was cased and cemented to the bottom with API 5" OD N 80 casing.

The holes were air-drilled. No water was encountered in drilling, and no water is present within the casings. Nipples were installed so that 1½ to 2 feet of casing are exposed above the surface with male threads up and protected with suitable caps.

Facilities

A rectangular concrete pad was poured around the three cased boreholes extending at least 5 feet horizontally from all holes. The site has been graded to provide a parking area for vehicles and trailers, and the road to the site from Pepper's main road has been graded and filled. The site is easily accessible by passenger car.

An adobe hut with approximately 15 ft. x 15 ft. of interior floor space has been constructed adjacent to the concrete pad. Electrical power (110 and 220 volt, single phase) was brought to the site. Three power drops were placed to serve the hut and at least two trailers. Telephone lines were strung (Big Bend Telephone Company) to provide a leased data line to Dallas (SMU campus) and a standard telephone.

A water line was laid from Pepper's main water supply to provide water for use in trailers and for fire protection. A drain system and septic tank was installed so that a camper-trailer could be placed on the site.

The site is now in operation with equipment installation being accomplished under an AFOSR-DARPA contract which began following the completion of the contract covered by this final report.

GEOPHYSICAL INVESTIGATIONS OF YUCCA FLAT, NEVADA

John F. Ferguson

ABSTRACT

In support of seismological studies of Yucca Flat, Nevada, a three-dimensional geophysical model has been produced. Information from geologic mapping, borehole stratigraphy and geophysics along with Bouguer gravity measurements have been combined to produce a map of the Tertiary-Paleozoic interface beneath the valley. This model has been applied to the interpretation of three seismic reflection profiles gathered specifically for this study. These data provide a measure of structural relief and fault distribution within the basin. The structure may be given a coherent geologic interpretation with respect to the tectonics of the western United States during the Cenozoic. The model can also provide a deterministic explanation for anomalous explosion magnitudes observed at Yucca Flat.

INTRODUCTION

In recent years it has become evident that lateral variations in geologic structure at Yucca Flat, Nevada, exert controls over the far field waveforms from explosions detonated there. A marked correlation was observed between structural contour, Bouguer gravity, and normalized body wave magnitude maps. This correlation suggested that a deterministic geophysical model based on an accurately defined geologic structure could be used to predict far-field body wave amplitude variations. When the examination of existing structural interpretations proved to be deficient, it was decided to obtain modern seismic reflection profiles. In addition, a reevaluation of the United States Geological Survey (USGS) gravity data used in earlier structural interpretations seemed to be appropriate. Various borehole and other geologic data were obtained from Los Alamos National Laboratory (LANL) and published sources to aid this research.

Yucca Flat, Nevada, is a graben-like structure of Cenozoic age. The underlying strata are mainly sediments of Paleozoic (Pz) age. Major volcanic centers to the west have introduced a thick sequence of tuff units which are generally less than 20 million years old (Tv). Within Yucca Flat and adjacent valleys alluvium of Quaternary age (Qal) covers the volcanics to a thickness of over 300 m. Major normal fault sets strike east-west, northwest-southeast and north-south. The last group are apparently the youngest and have a substantial strike slip component of motion. This brief geologic description will be expanded after introduction of the geophysical model.

The interpretative procedure used from the outset of this study required the examination of as many different types of data as possible in order that the resulting model be a complete explanation of the basin phenomena, consistent with all observations. In particular, gravity observations, borehole data and seismic reflection profiles were simultaneously used in the interpretative process. It was also found that the structure must be modeled in three dimensions to achieve reliable results.

This report presents the resulting three dimensional geophysical model for Yucca Flat. Results of numerical wave propagation experiments will be presented in a later report directed toward the seismological aspects of this study.

GEOLOGIC INFORMATION

Geologic maps produced by the USGS and compiled at a 1:24000 (7.5 minute quadrangle) scale were available for the entire study area. These are map sheets GQ 213,214,215,363,384,577,582,746,and 1327. The geologic base map upon which the geophysical data are compiled is derived from these maps. Additional geologic maps and data have become available from LANL and USGS sources concerned with the Nevada Test Site (NTS). The Geological Society of America Memoir 110, Nevada Test Site, edited by Eckel (1968) contains a great deal of pertinent information.

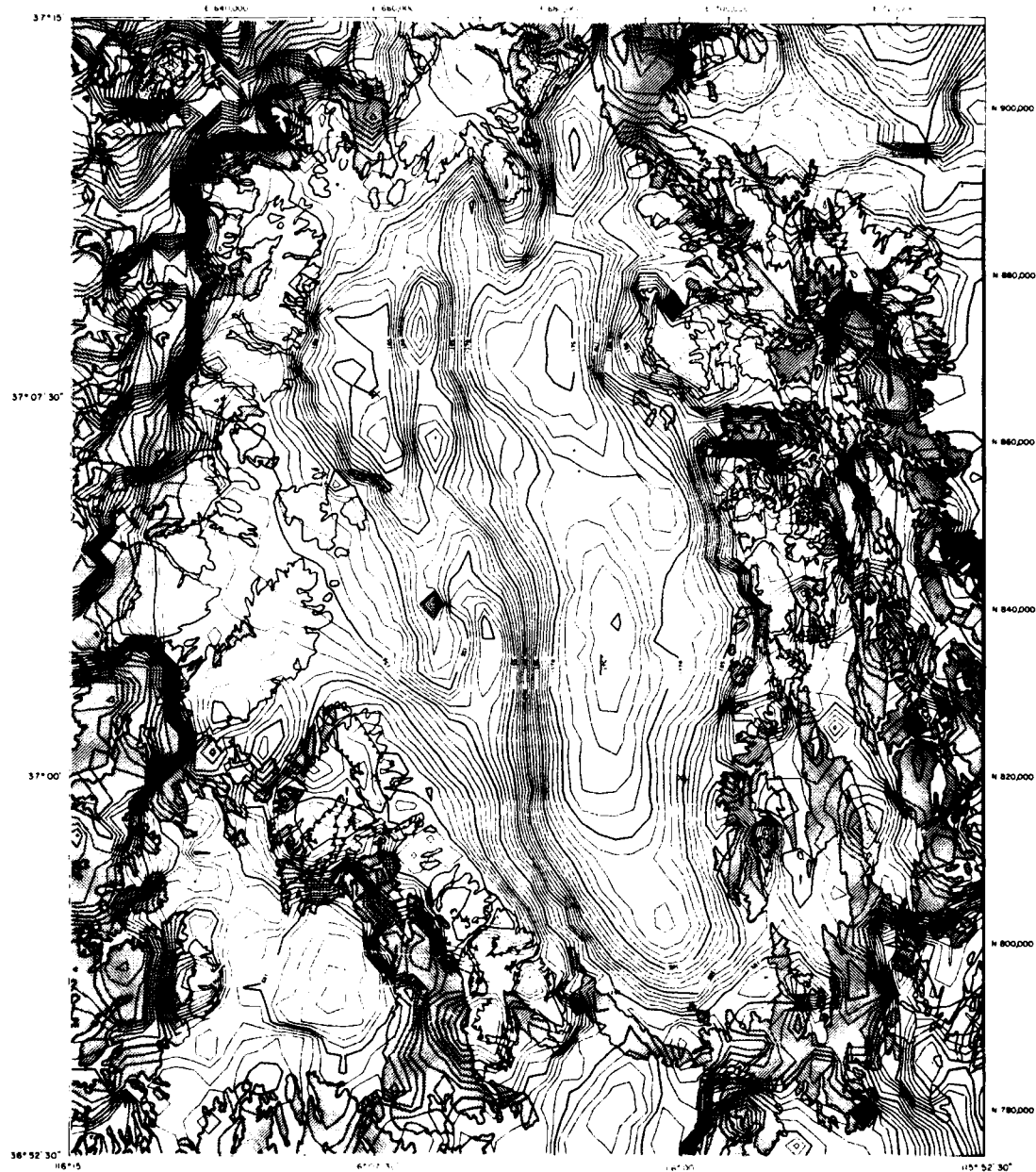
Borehole stratigraphic and geophysical data have been of particular importance. Most of the borehole data were obtained from LANL; consequently, only limited data from areas managed by Lawrence Livermore Laboratory (LLL) or from areas that are of little interest to either group. The borehole geophysical data consist of summaries compiled by LANL of average properties for various stratigraphic units. In some cases the original logs were available. There are 36 such boreholes summarized, including 7 which penetrate to the Paleozoic, 17 which penetrate into the Tertiary, and 12 which bottom in the Quaternary alluvium. In addition we have examined borehole gravity data for 41 holes in Yucca Flat. Control on the Paleozoic surface is provided by the 90 holes shown in figure 1. The alluvium-volcanic contact is controlled by a total of 166 holes. These holes are not the complete

Fig. 1. Location map of boreholes contacting the Paleozoic Basement used in this study. The numerical portion of the borehole designation corresponds to area designations used in some sections of this dissertation. The geologic base map will be used in all subsequent maps. The dark shade represents Tertiary volcanic rocks, the light shade represents Quaternary alluvium and the white areas are Paleozoic outcrop. The Climax stock in the northern part of the map is stippled. Nevada Central Zone coordinates in units of feet are provided.

GRAVITY DATA

Some 8459 gravity stations are located within an area 22.5 minute on a side around Yucca Flat. The data are from USGS open files and were collected over a twenty year period by various people using different instruments. Most of these data, 6383 stations, are within Yucca Flat. Of the remainder, 351 are sited on Paleozoic outcrops and 1725 are in neighboring basins and on the volcanic outcrops which border the basins. The magnetic tape file containing this compilation specified location to 0.01 minute, elevation to 0.1 foot and terrain corrected Bouguer anomaly to 0.01 milligal. The precision and quality of these data are variable. An accuracy of estimate of ± 0.5 milligal is assumed for the overall data set, although the newer data is probably good to ± 0.15 milligal (Felch, 1979). Figure 2 is a contour map of this Bouguer gravity data.

Fig. 2. Complete Bouguer anomaly map of the Yucca Flat, Nevada area. The contour interval is 1 milligal.



YUCCA FLAT
NEVADA

ANALYSIS OF THE GRAVITY DATA

The abundant gravity observations (over 8000 stations) in a properly devised gravity inversion, constrained by the more sparse geologic and geophysical data, should produce a relatively detailed geophysical model. The model geometry most appropriate in this case is that of a basin of low density fill overlying a higher density half space. The shape of the model's lower perimeter will be sought as a function of position using the observed gravitational acceleration. The upper boundary is the earth's surface, which is known in advance. If the density distribution is also known, the interface shape is uniquely determined (Smith, 1961), for an infinite number of accurate observations. A finite and inaccurate data set will in general not permit a unique solution, but some average model can always be found. The inverse gravity problem for model shape is nonlinear and can be performed iteratively by techniques such as Gauss-Newton or successive approximations.

There exist many published inversion methods which have differing strengths and weaknesses in a given context. There is no perfect inversion theory of universal applicability. The following criteria were considered in the choice of an inversion routine:

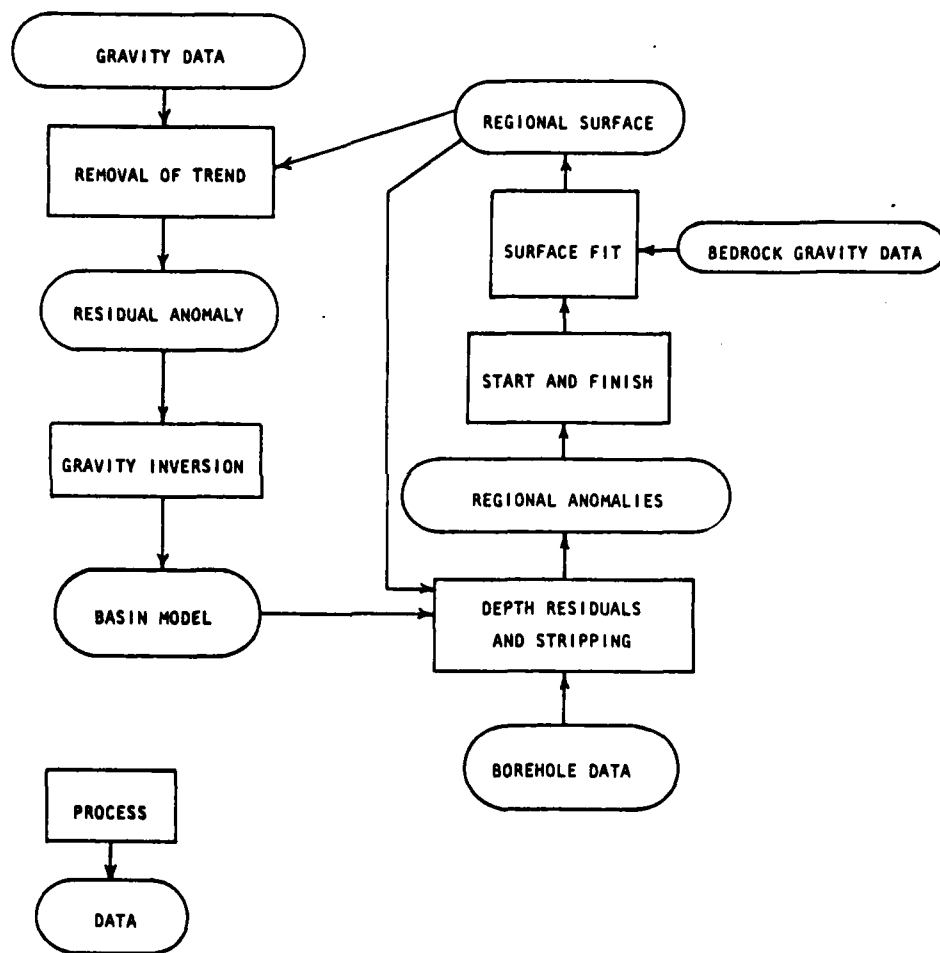
- 1) Ability to recover a best fitting solution (according to some norm).
- 2) Ability to assess the accuracy of the solution.
- 3) Ability to include a priori geologic and statistical information.
- 4) Speed and computer memory requirements necessary to invert thousands of observations.
- 5) Provision for a three dimensional model and variable density contrast, if necessary.

Trial and error methods were rejected as too crude. Initially some thought was given to vertical prism parameterization and linearized inversion similar to the technique of Burkhard and Jackson (1976). Preliminary experiments indicated that although this technique satisfied most of the criteria, the speed and memory economy were insufficient to be practical for the large data set. In addition, discrete parameterizations tend to produce models which are rather dependent on the parameterization (i.e., block size and location). An example of a block parameterized model based on these same data is contained in Felch (1979) who applied the Cordell and Henderson (1968) method to the Yucca Flat data.

An integral equation formulation of the problem could be specified which would overcome at least some of these problems. The interface would be represented by a continuous function of the spatial coordinates. A prototype program of this sort was written for two dimensional basin models which worked quite well. Results of that program were presented by Goforth, et al. (1979). However, this experience indicated that computational limitations would rule out a three-dimensional implementation of that technique. The method finally selected is similar in some respects to the integral equation formulation. It is the Parker-Oldenburg-Huestis method (Parker, 1972, Oldenburg, 1974, Parker and Huestis, 1974), which uses Fourier expansions to achieve computational speed through application of the fast Fourier transform. The details will be discussed in a later section.

In a local study the regional gravity anomaly is really part of the model specification. It is that part of the field which is not accounted for by the model in question and usually is arbitrarily parameterized. We choose to specify the regional gravity by a low-order Fourier trend surface, which is fit to those gravity stations occurring on the Paleozoic outcrop (i.e., the half space of the model). Additionally, the estimation of this anomaly is made a part of the inversion process by removal of the modeled basin gravity effect at the borehole Pz control points within the basin and the use of the resulting anomalies in the least squares surface fitting. This concept was applied to Yucca Flat by Felch (1979). The notion has been extended in this application to a procedure which iteratively improves the regional gravity estimate. Starting with a surface with no borehole control, the residual anomaly is inverted. The depth residuals at the boreholes are used to correct the stripping of the basin anomaly, a new regional anomaly surface is better defined. It is possible that long wavelength variations in density contrast, if improperly specified, will be confounded with the regional anomaly produced by this process. A simplified flow chart of the entire procedure is presented in figure 3. Each box is a separate computer program which operates on various intermediate data files. The process may be cycled as many times as necessary to achieve stable error statistics.

Fig. 3. Flow chart depicting the major elements of the gravity interpretation procedure. The rectangular boxes represent processes performed by computer programs and the elliptical boxes represent data files both generated and operated on by the programs.



THE PARKER-OLDENBURG-HUESTIS
POTENTIAL INVERSION

Parker (1972) devised an expansion of the integral equation for the gravitational (or magnetic) potential in the form of a series of Fourier transforms. In the following we define the z-axis to be positive downward. The anomalous potential is assumed to be due to a layer of contrasting density and variable thickness, which vanishes outside of some finite area, D, and is specified by

$$1) \quad U(\vec{r}_0) = G \int_D \int_{h(\vec{r})}^{g(\vec{r})} \frac{\rho(\vec{r})}{|\vec{r}_0 - \vec{r}|} dz dS,$$

where $g(\vec{r})$ and $h(\vec{r})$ are the lower and upper surfaces of the layer. The potential is observed on a plane, z_0 , above the layer at all points and in finite domain, X. We may Fourier transform equation 1,

$$\begin{aligned} 2) \quad \mathcal{F}[U(\vec{r}_0)] &= \int_X U(\vec{r}_0) \exp(i\vec{k} \cdot \vec{r}_0) dS_0 \\ &= G \int_D \int_{h(\vec{r})}^{g(\vec{r})} \frac{\rho(\vec{r}) \exp(i\vec{k} \cdot \vec{r}_0)}{|\vec{r}_0 - \vec{r}|} dz dS dS_0. \end{aligned}$$

The integrals over X and z can be performed analytically to produce

$$\begin{aligned} 3) \quad \mathcal{F}[U(\vec{r}_0)] &= 2\pi G \int_D \rho(\vec{r}) \exp(i\vec{k} \cdot \vec{r} + |\vec{k}| z_0) \\ &\quad \cdot [\exp(|\vec{k}| (h(\vec{r}) - g(\vec{r}))) / |\vec{k}|^2] dS. \end{aligned}$$

The vector \underline{r} is the projection of \underline{r} onto the plane z_0 . Parker then expands the second exponential in a Taylor series and exchanges the order of summation and integration resulting in the rather novel representation of the potential spectrum as an infinite series of Fourier transforms,

$$4) \quad \mathcal{F}[u(\vec{r}_0)] = -2\pi G \exp(|\underline{k}|z_0) \sum_{n=1}^{\infty} \frac{|\underline{k}|^{n-2}}{n!} \mathcal{F}[\rho(\underline{r})(h^n(\underline{r}) - g^n(\underline{r}))]$$

The potential may be differentiated with respect to z to obtain the gravitational acceleration. Equation 4 can be rearranged slightly into a remarkable triplet of formulas:

$$5a) \quad \mathcal{F}[\Delta g(\vec{r}_0)] = -2\pi G \exp(|\underline{k}|z_0) \sum_{n=1}^{\infty} \frac{|\underline{k}|^{n-1}}{n!} \cdot \mathcal{F}[\rho(\underline{r})(h^n(\underline{r}) - g^n(\underline{r}))],$$

$$5b) \quad \mathcal{F}[\rho(\underline{r})] = \frac{-\mathcal{F}[\Delta g(\vec{r}_0)] \exp(-|\underline{k}|z_0)}{2\pi G \mathcal{F}[h(\underline{r}) - g(\underline{r})]} - \sum_{n=2}^{\infty} \frac{|\underline{k}|^{n-1}}{n!} \cdot \mathcal{F}[\rho(\underline{r})(h^n(\underline{r}) - g^n(\underline{r}))],$$

$$5c) \quad \mathcal{F}[g(\underline{r})] = \frac{-\mathcal{F}[\Delta g(\vec{r}_0)] \exp(-|\underline{k}|z_0)}{2\pi G \mathcal{F}[\rho(\underline{r})]} - \sum_{n=2}^{\infty} \frac{|\underline{k}|^{n-1}}{n!} \cdot \mathcal{F}[\rho(\underline{r})(h^n(\underline{r}) - g^n(\underline{r}))],$$

Now 5a states the forward problem of finding the gravitational field given the density and layer shape. Equation 5b states the linear

inverse problem of the determination of density given gravity observations and layer geometry, and 5c states the nonlinear inverse problem for layer shape given the gravity data, density, and upper surface. The geophysical model of a basin would have fixed upper and variable lower surfaces. Variation of the upper surface, with a fixed lower surface, could model an intrusion. The inverse problems may be solved by successive approximations given some initial guess for $g(\underline{r})$ or $\rho(\underline{r})$. In this approach the correction to the function guess is a nonlinear step at each iteration and hence has some desirable properties relative to the linearized inversion schemes currently popular. In addition, for N observations the Fourier integrals may be computed in $N \log(N)$ operations for gridded data, whereas the integral equation methods require order N^3 operations for the decomposition of a system of linear equations.

Notice that the leading, linear term of the expansion in equation 5 is merely the continuation operator in the wavenumber domain. To first order the method is equivalent to Peters' method (Peters, 1949 and Gunn, 1975) for the interpretation of gravity and magnetic data, which has been in use for nearly fifty years. This now classic technique applied a downward continuation operator in the space domain to obtain a surface density distribution at depth called an equivalent stratum. For a constant density contrast the density variations on the equivalent stratum translate into topography on a surface about the depth of continuation. The linearized method requires that the topography be very small relative to the depth. Parker's technique adds in the higher order terms as necessary to provide convergence for arbitrary topography.

Some important results on series convergence and other properties are given by Parker (1972), Parker and Huestis (1974), and Oldenburg (1974). A discussion of this theory from the standpoint of integral equations may be found in Dorman and Lewis (1974) and in a similar derivation from the Russian literature in Tsirul'skiy (1968) and Tsirul'skiy and Ospischeva (1968).

A rather serious problem in the two inversion formulas arises from the downward continuation operation. Downward continuation is an ill-posed problem; that is, any small perturbation of the gravity field, such as that due to noise in the data, may result in an unbounded perturbation in the continued field. Some form of regularization or smoothing is essential to bound for the solution of such problems. This is particularly important in nonlinear problems when the inverse mapping is approximate. Parker, Oldenburg and Huestis have used a rather arbitrary low-pass filter to eliminate short wavelengths from the solution, but our experience shows that this is not a satisfactory approach. A better filter derives from the work of Tikonov (1963). A regularization is defined as

$$6) \min [M_{\alpha}(m)] = \min \left[\int (U(r) - A(r, m))^2 dr + \alpha \|m(r)\| \right].$$

The operator, A , defines the forward problem, where $U(r)$ is the observed data, and $m(r)$ is the approximate function sought. The first term is the data misfit and the second is some measure of model smoothness. The parameter, α , will be called the regularization

parameter; it controls the smoothing in the inversion for the approximate model. The first error term will never be zero but can be made quite small with a proper choice of a regularized inverse operator.

In Tikhonov et al. (1968) several approximate inverses for the downward continuation problem are given. The function,

$$7) \quad A(k) = 7 [\Delta g(\vec{r}_0)] \exp(-|k|z_0) / (1 + \alpha |k|^2 \exp(-|k|z_0)),$$

was selected as most suitable for this purpose. It has the form of a smooth low pass filter which cuts off a faster rate than the downward continuation operator grows. The regularization parameter, α , is chosen by forming a family of approximate inverses by varying α in a systematic way, testing each one by forward calculation and computing the rms error between the theoretical and the observed accelerations. The simplex procedure of Nelder and Mead (1965), as presented by O'Neil (1971), provides a convenient method for this minimization. In one dimension (the α dimension) the simplex is a line segment which attempts to bracket the minimum. This line segment will flip back and forth and expand or contract as necessary to obtain the minimum. Convergence is reached when the segment shrinks below a certain length.

Unlike the methods based on linearized solutions to the integral equations, the Fourier transform method does not produce the Frechet derivatives as a by-product. This complicates the calculation of Backus-Gilbert linear resolving kernels. Parker and Huestis (1974) offered an approximate resolving measure for the linear inverse problem (5b), but it performed poorly. The resolving widths were larger than the model even for the highest variance solutions. The space domain

width of the regularizing filter provides some information on resolution, but it lacks the space variable quality of the Backus-Gilbert resolution measures. Because of the lack of a linear mapping it is also difficult to compute model variance. It is conjectured that the magnitude of the variance could be inferred by consideration of the terms which are suppressed by regularization. Acknowledging these difficulties the error analysis utilized here will be based on the errors between the model and known (borehole) depths.

THE DENSITY MODEL

The geophysical model proposed here consists of a Paleozoic half space with a lower density basin with Cenozoic age fill on top. The density contrast could have any manner of spatial variability. The simplest density distribution one can assume in order to model the basin would be a single constant density contrast across the interface between the Cenozoic and Paleozoic strata. However, in the Great Basin it is common to encounter density functions which increase more or less exponentially with depth. Cordell (1979) has proposed that lateral variations, with density decreasing toward the basin center may be important. Some basis for the choice of a density model must be found in the observed density data.

For many years a constant density contrast, between the Cenozoic and Paleozoic rocks, of -0.7 gm/cc has been the standard model for Yucca Flat (Hazelwood, et.al., 1963, Healey, 1966 and 1968). It has also been recognized that there are departures from this average, but the importance of the departures has not previously been determined. Density log information from 34 boreholes was used in a simple statistical analysis of this question. This information is from a zone extending from roughly the center of the valley to the eastern margin and covering about the middle fourth. It is questionable how representative of the remainder of the valley these densities may be. Table I

TABLE I
BOREHOLE DENSITY STATISTICS FOR YUCCA FLAT, NEVADA

GEOLOGIC UNIT	NUMBER OF SAMPLES	MEAN	STANDARD DEVIATION	MEDIAN	INTERQUARTILE DEVIATION	MIDRANGE	RANGE
QAL	34	1.77	0.16	1.77	0.10	1.84	0.72
TV	123	1.79	0.19	1.81	0.12	1.90	1.06
PZ	3	2.47	0.32	2.45	0.54	2.48	0.64

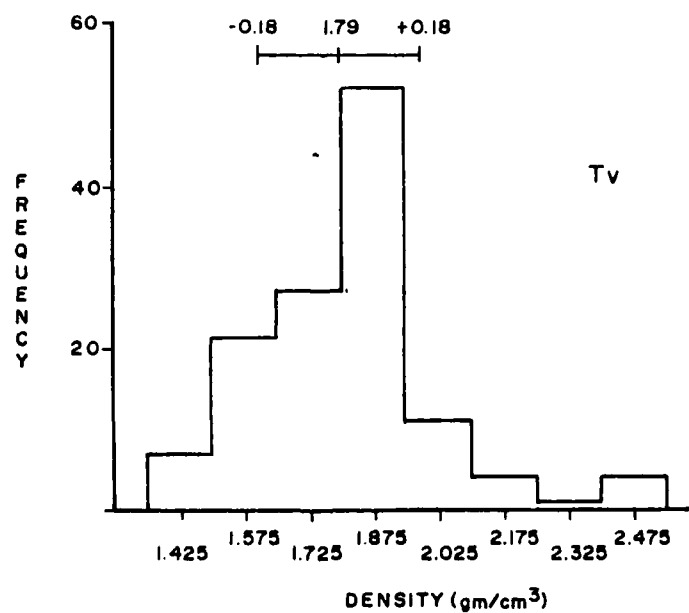
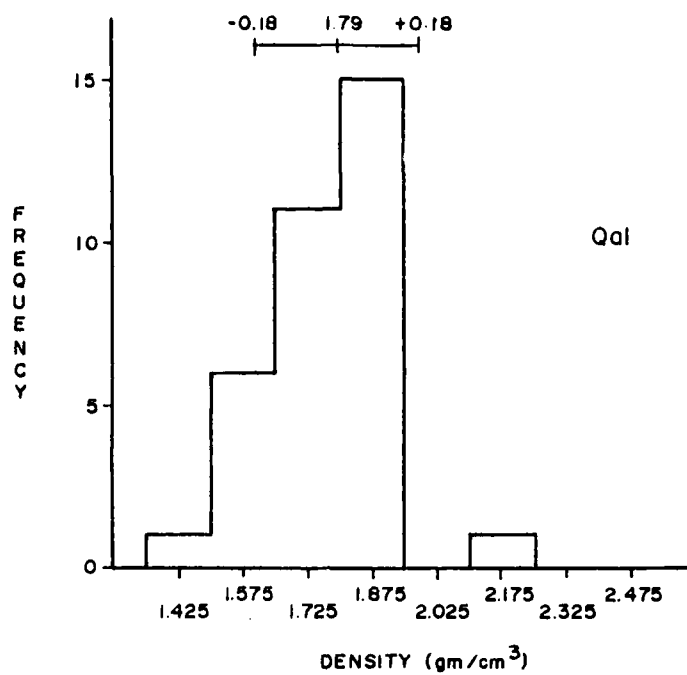
UNITS ARE G/CC

summarizes the statistics on the geologic units Qal, Tv, and Pz. A t test for the equality of the means of the Qal and Tv population was performed with the conclusion that the means were equal at the 90% confidence level. The mean and standard deviation of the combined population are 1.79 gm/cc and 0.18 gm/cc. Figure 4 is a plot of the histograms of the Qal and Tv samples with the normal distribution parameters (mean and standard deviation) for the combined population superimposed. The frequency distributions are not normal and are skewed towards the low density end. A major deficiency in this analysis is the lack of volumetric weighting of the density values. Samples from thin layers are given equal weight with samples from thick layers. The conclusion is that the Qal is indistinguishable from the Tv in density, and hence only one layer of fill with no vertical density variation need be considered for the valley model. The quality of the summary data from density logs probably does not warrant a more detailed analysis.

Better data for the purpose of density modelling can be obtained from the borehole gravity logs. Borehole gravity provides a better average density for the area around the hole than density logs which may be complicated by local borehole effects; however, lateral variations in structure may bias the gravity results. The borehole gravity logs which start at depths of less than 200 meters and extend to depths greater than 500 meters were selected from the 41 logs available. The derived density and the average density were plotted as a function of depth. The latter function is more useful because it rectifies the data and suppresses the effect of thin, anomalously

Fig. 4. Histograms of the occurrence frequency of density values for all stratigraphic units in the Quaternary (a) and Tertiary (b) rocks of Yucca Flat. The data were compiled from interval density estimates from the central latitude portion of the valley. The bar scale at the top of each graph shows the mean and one standard deviation fiducials for the combined distribution.

DENSITY STATISTICS YUCCA FLAT, NEVADA



dense, layers. When the average density curve changes slope, it indicates a profound density change. A comparison of the Yucca Flat average density profile and those of several other western localities in the United States are shown in figure 5. The comparison illustrates the unusual nature of the Yucca Flat distribution. The Yucca Flat curves are rather constant with depth and show little evidence of a significant exponential increase in density with depth; many curves even show a decrease in density with depth. The limits drawn on the graph are the mean and standard deviation from the geophysical log distribution. Although lateral variation is present it is generally less than ± 0.1 gm/cc and no systematic variation is apparent.

The density of the Paleozoic basement is less well determined. Some samples have been tested in the laboratory and some geophysical data exist. The choice of 2.5 gm/cc seems to be justified by these data. Lateral variations are known to exist, but we have insufficient information to characterize them. These observations support a constant density contrast model of -0.7 gm/cc. With more data, variations of ± 0.1 gm/cc could be included in the model, but this is probably unnecessary for this study.

Fig. 5. (a) is a plot of average density as a function of depth for Yucca Flat, Nevada and (b) shows the same data for several other representative localities in the Basin and Range province. All density estimates are from borehole gravity measurements except those in Hachita and Sulphur Springs valleys. The fiducials lines drawn vertically on the left graph are the mean and one standard deviation, derived from the Quaternary and Tertiary density data used in Table I.

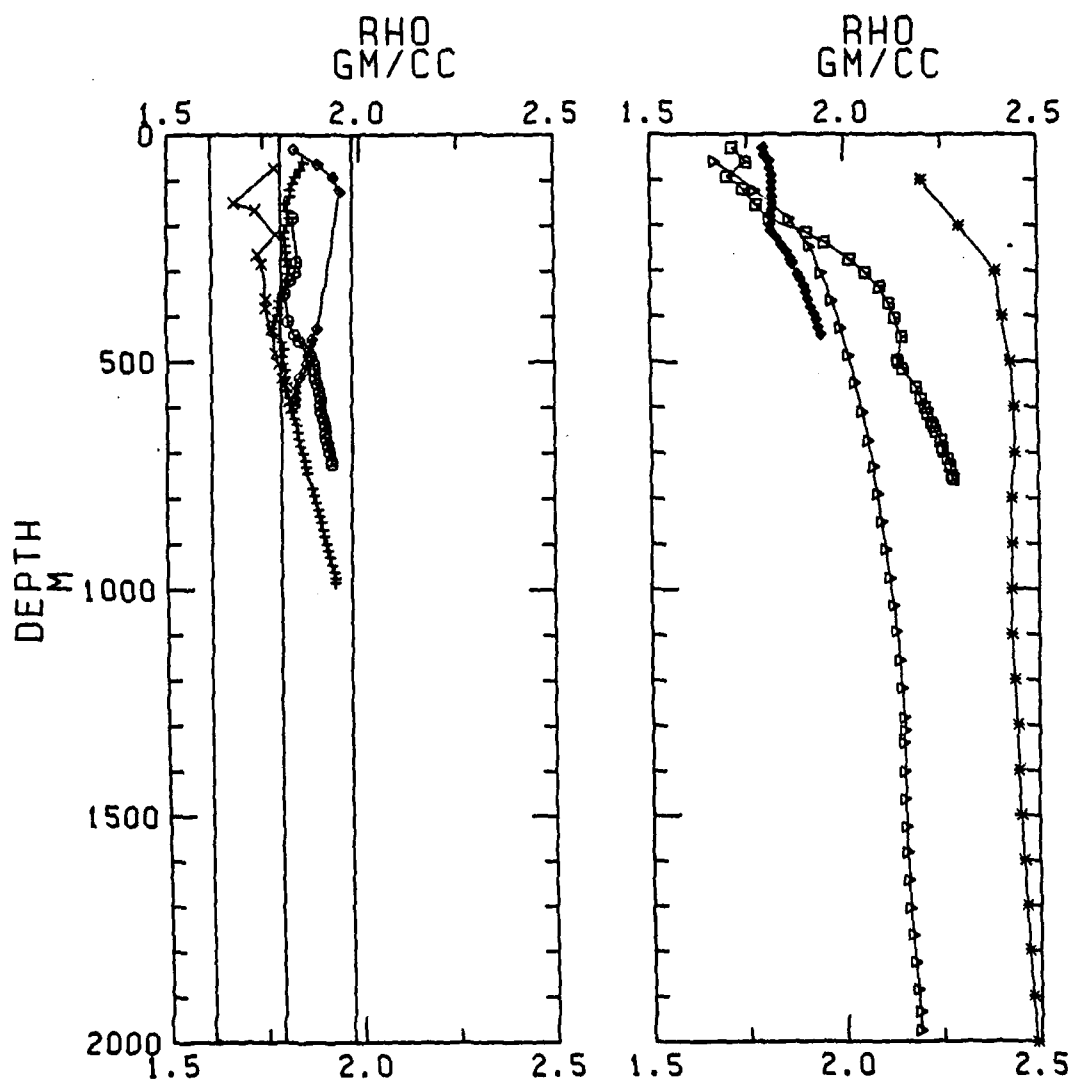
AVERAGE DENSITY VS DEPTH FUNCTIONS

YUCCA FLAT, NEVADA

- U2EI
- + U4E-1
- x U7AP
- o U7AU

OTHER BASIN AND RANGE AREAS

- FRENCHMAN FLAT, NEVADA
- * HACHITA VALLEY, CHIHUAHUA
- ▷ HOT CREEK VALLEY, NEVADA
- ◻ SULPHUR SPRINGS VALLEY, ARIZONA



THE GRAVITY MODEL

As outlined previously a gravity interpretation scheme employing the Parker-Oldenburg technique formed the heart of the structural interpretation. A basin model was estimated in conjunction with the regional anomaly. The density function was specified a priori. Ninety boreholes were used as intrabasin control points. The gravity field and the interface were specified on a rectangular grid with the y-axis north and the x-axis east. The grid is specified by 76 x nodes, 65 y nodes, 1600 feet x spacing, 2000 feet y spacing and origin 620000 E and 780000 N in the Nevada central zone coordinate system (units are feet). The gridding is required for efficient computation of the Fourier integrals in the inversion process using the fast Fourier transform. Since the density was assumed to be homogeneous in the basin it was not specified on a grid as it otherwise would have been. The gridding was accomplished by use of Shepard's bivariate interpolation function (Shepard, 1968) combined with a rapid search technique adapted for the high data density (6383 stations) encountered at Yucca Flat. Some smoothing is inherent in the gridding, which helps to suppress aliasing and high frequency noise in the grid.

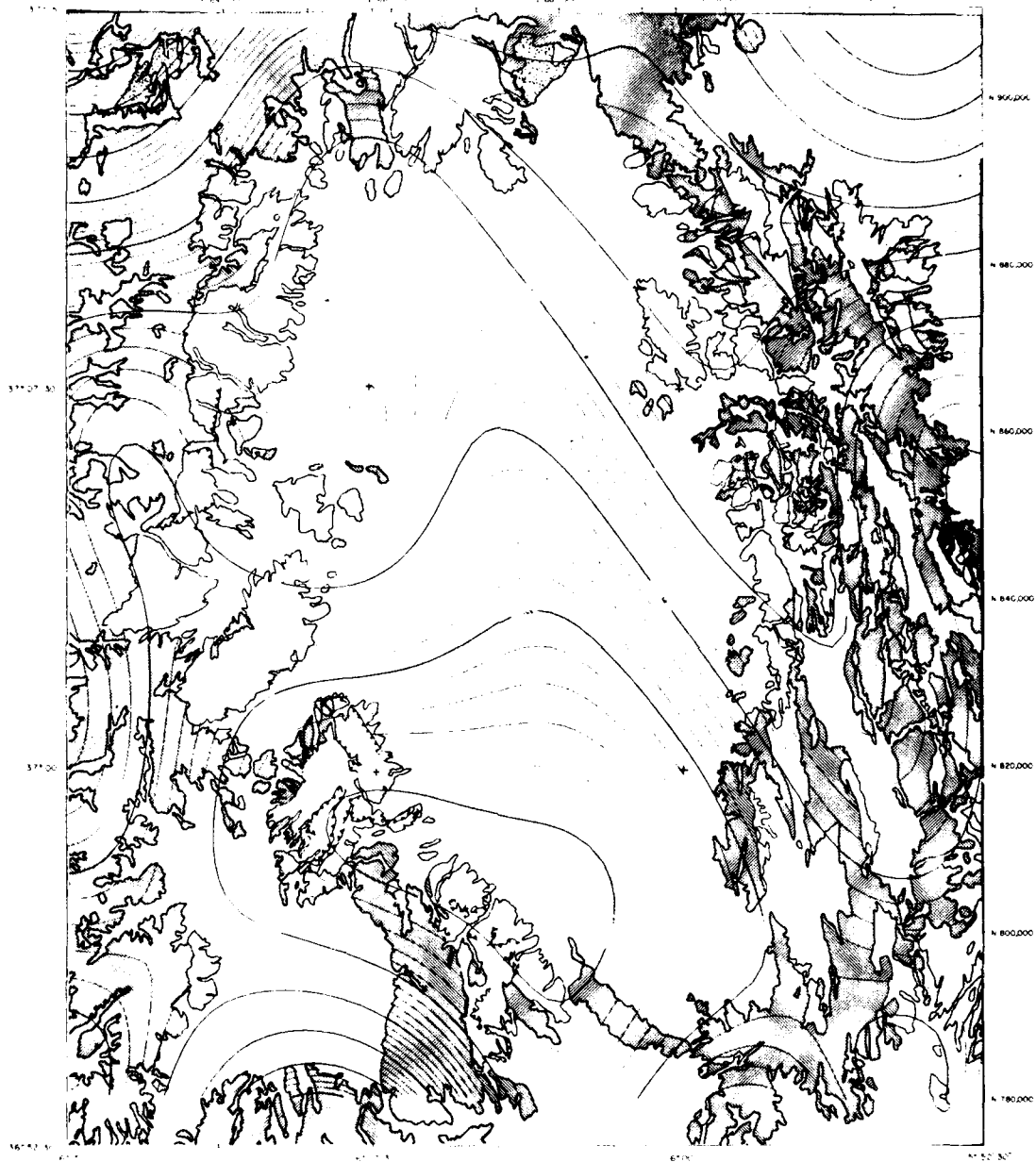
Proper determination of the regional gravity anomaly is of particular importance at Yucca Flat. Inspection of small scale Bouguer anomaly maps of the western United States, such as Eaton, et al.,

(1978), reveal that the valley sits astride a high ridge extending north from the California border. Just to the northwest, a large volcanic caldera complex produces a large, circular low which truncates this trend. The locally-defined regional anomaly should account for this gravity ridge.

The regional anomaly was defined by a low order Fourier surface of two harmonics (25 terms). The fundamental wavelengths of 100000 feet east to west and 220000 feet north to south are roughly twice the basin dimensions. This surface was computed by least squares fit to 350 gravity stations, which occur in areas of Paleozoic outcrop, and gravity anomalies corrected for the basin effect at the 90 borehole locations in Yucca Flat. The data from stations and holes were weighted so that both groups of data would provide approximately equal effects on the resultant surface. The regional anomaly is displayed in figure 6. This map shows the ridge and part of the expected circular depression. The anomaly is gently convex upward. If it were not, and linear gradients were employed as is common practice, the depth would be substantially underestimated.

The residual anomaly at each iteration was multiplied by an areal rectangular truncation window of highly irregular shape, which was somewhat larger than the basin itself but smaller than the total grid. To the extent that the regional separation removed the effect of the half space of the model, a satisfactory taper was achieved. In the southeast corner of the basin the Paleozoic rocks do not outcrop and hence a fundamental assumption of the model is violated. The residual

Fig. 6. The regional gravity anomaly used in the calculation of the final depth model. A low order Fourier trend surface was fit to gravity stations on the Paleozoic outcrop and estimated anomalies at the borehole control points shown in figure 1. The contour interval is 1 milligal.

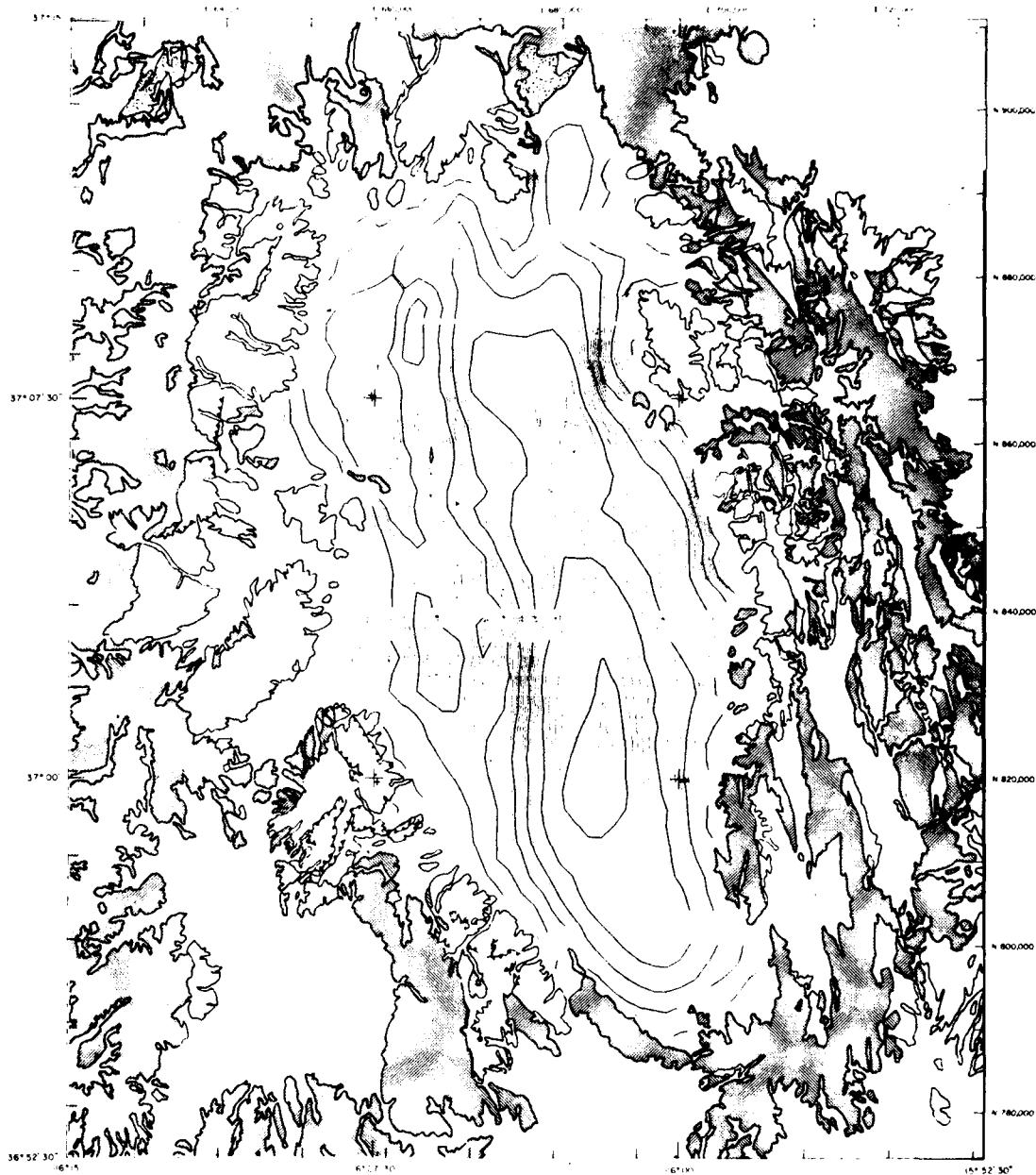


YUCCA FLAT
NEVADA

does not taper and is abruptly truncated by the window. The resulting Gibb's oscillations do not seem to be significant within the basin. In future calculations a better window will be developed. The residual which was invented for the final model is mapped in figure 7.

In each iteration of the interpretation process (see figure 3) the error statistics at the boreholes were monitored. After six iterations no real improvement in the fit was obtained and the procedure was terminated. The final model is referred to as F1B and is shown in figure 8. The gravity misfit, as shown in figure 9, is acceptably low over the deeper parts of the basin and increases slightly in the shallow areas. The error statistics are summarized in Table II; histograms of the gravity data misfit and borehole misfit are provided in figure 10. The distributions are not Gaussian and have some very significant outliers. The rank order statistics, the median and inter-quartile deviation, are much more reliable estimates of location and scale in this case. The model thus satisfies the data within ± 0.5 mgal with some negative bias. The borehole depth mismatch is biased slightly positive which would agree with the data error. The borehole data have several known mislocations and some ambiguity in the definition of the Paleozoic contact is introduced by a thick colluvium on the Paleozoic rocks. The stated borehole depths do not always agree with the modeled depths due to this ambiguity. It should also be remembered that the model depths are really spatial averages and not point measurements like the boreholes. The basement depth deviation would be robustly estimated to be ± 80 m, which represents about a 15% error on the average. These statistics are in good agreement with Felch (1979).

Fig. 7. The residual gravity anomaly, which results from the subtraction of the regional anomaly in figure 6 from the Bouguer anomaly in figure 2. The contour interval is 1 milligal.

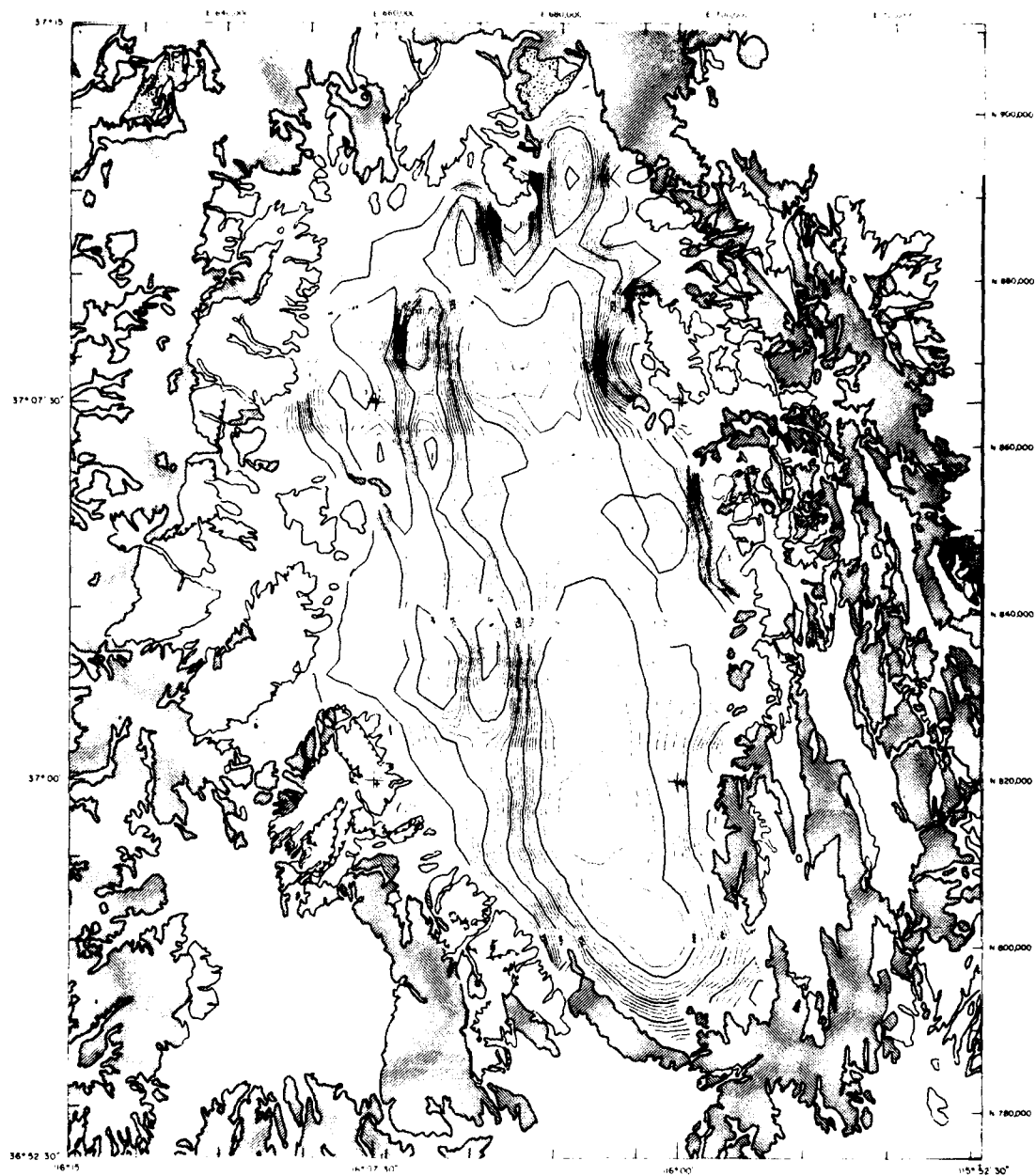


YUCCA FLAT
NEVADA

KILOMETERS

MILES

Fig. 8. The Tertiary-Paleozoic contact depth model for Yucca Flat, Nevada, designated F1B. Note the deep low areas on the east and the shallow lows on the west separated by a horst. The contour interval is 100 meters.



YUCCA FLAT
NEVADA

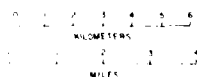
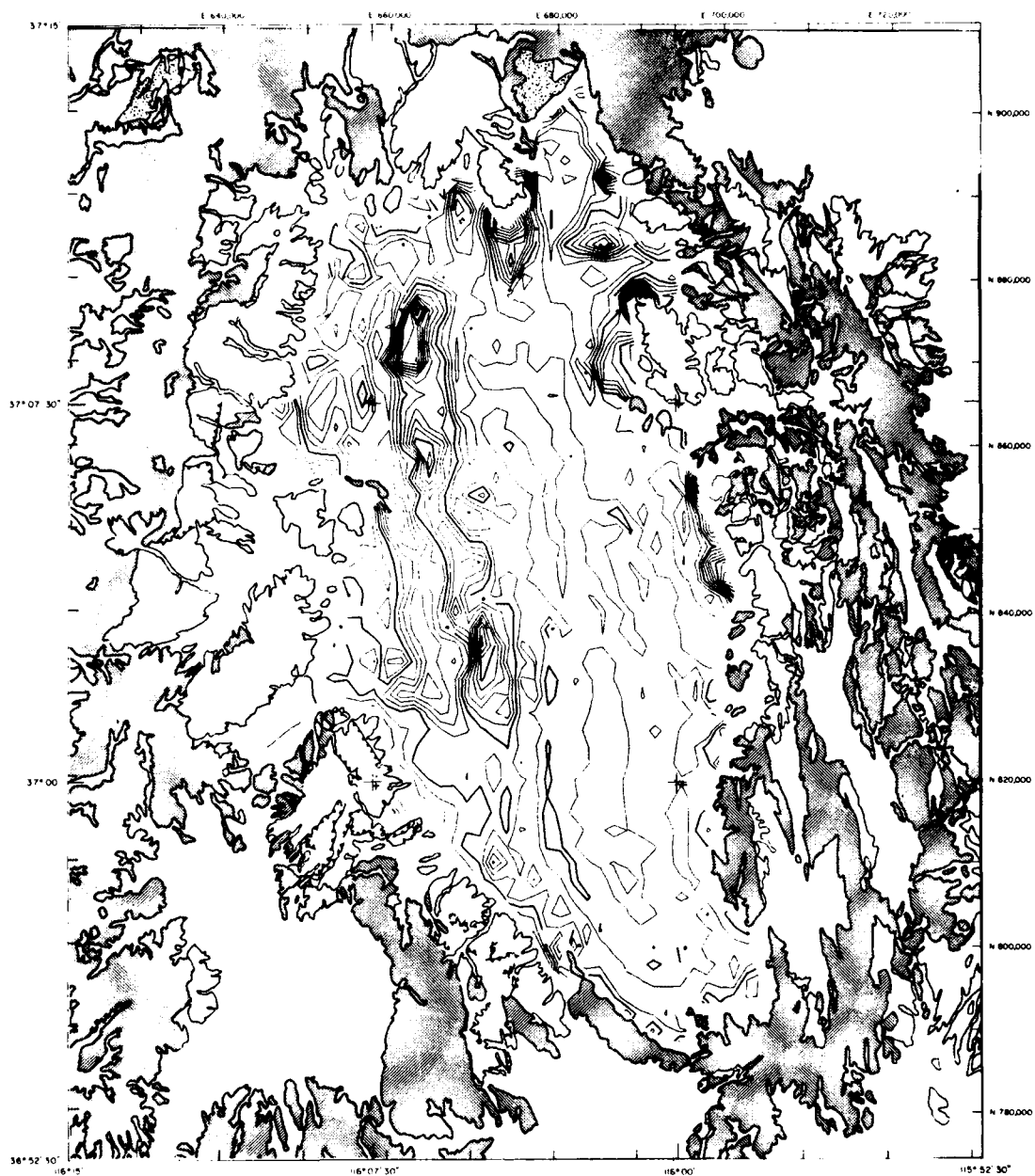


Fig. 9. The error between the residual Bouguer anomaly of figure 7 and the theoretical anomaly computed from the model in figure 8. The contours are in units of 0.5 milligal. The error is less than 1 milligal except in shallow areas near the basin margins and over the horst.



YUCCA FLAT
NEVADA



TABLE II

ERROR STATISTICS FOR MODEL F13 YUCCA FLAT, NEVADA

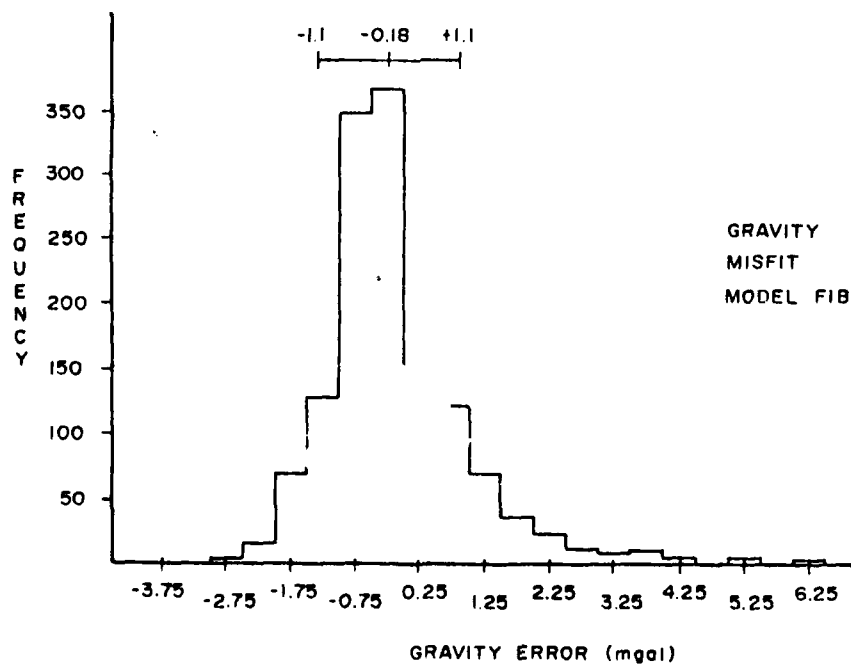
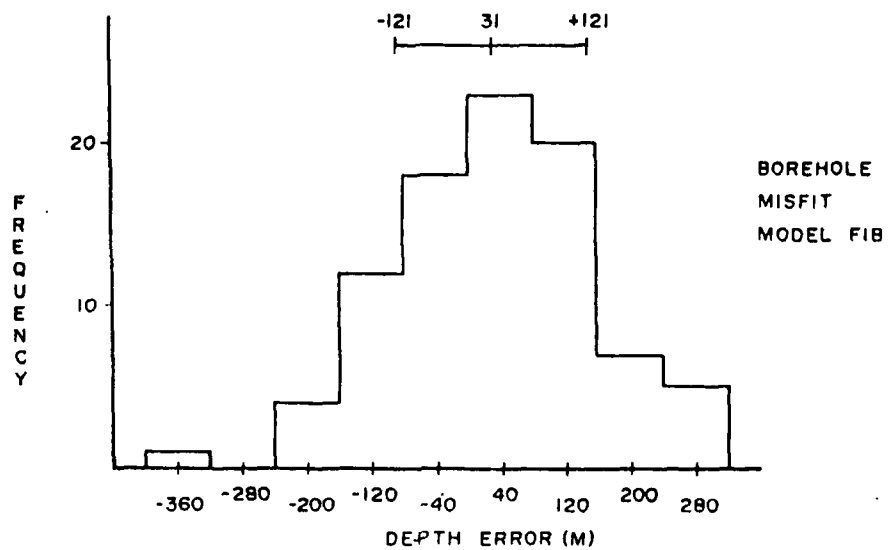
DEPTH MISFIT AT 90 BOREHOLES IN KM

MEAN = 0.031
STANDARD DEVIATION = 0.121
ROOT MEAN SQUARE = 0.125
MEDIAN = 0.026
INTERQUARTILE DEVIATION = 0.033
QUARTILE COEFFICIENT OF SKEWNESS = -0.03

GRAVITY MISFIT AT 1336 GRID NODES IN MGAL

MEAN = -0.18
STANDARD DEVIATION = 1.10
ROOT MEAN SQUARE = 1.12
MEDIAN = -0.39
INTERQUARTILE DEVIATION = 0.49
QUARTILE COEFFICIENT OF SKEWNESS = -0.69

Fig. 10. (a) shows the frequency of depth error values in meters at the borehole locations on figure 1 for the model shown in figure 8. (b) is a histogram of gravity misfit errors at the grid nodes within Yucca Flat which are contoured in figure 9. The fiducial limits of one standard deviation about the mean are placed above both histograms.

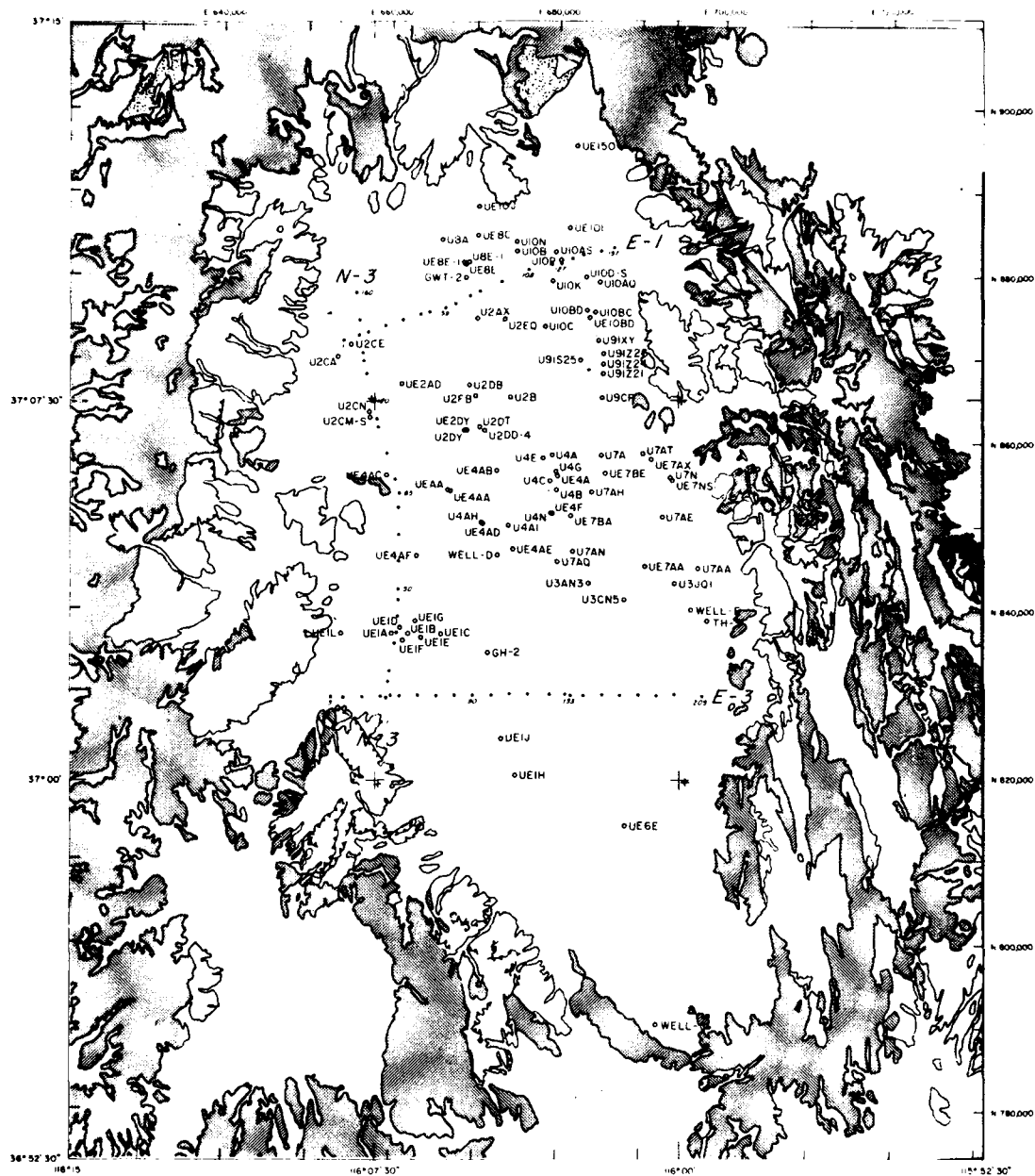


This model is only a first effort and has limitations on it which are rather artificial at this time. In the Yucca Flat area over 6000 gravity stations are available and only 1300 grid nodes occur in the same area. Thus, the data grid could be considerably refined. About 100 borehole gravity soundings are available in addition to a selection of density logs. These data could be used to construct a laterally and vertically variable density function which would undoubtedly improve the fit in some areas. In addition some technical improvements to the algorithm especially in the areas of windowing, regional surface fitting and model regularization criteria are possible. These limitations in the data processing result in a decreased resolution and increased smoothness compared to what is actually possible using the available gravity data.

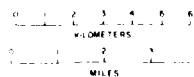
SEISMIC REFLECTION PROFILES

Three seismic reflection lines, one oriented north to south designated N-3, and two east to west, labeled E-1 and E-3, were recorded in January 1978. The locations of the lines are shown in figure 11. Four Y-900 vibrators provided sweeps of 8 to 32 Hz for 18 sec on N-3. Sweeps of 6 to 32 Hz for 12 sec were used on lines E-1 and E-3. Low frequency (4.5 Hz) geophones were used with 330 foot group intervals on N-3 and 220 foot group intervals on the east to west lines. All lines had 24-fold coverage. The north to south line, which was oriented parallel to the strike in an area with generally thin alluvial cover, was intended to recover deep crustal reflections, if possible. A more detailed description of the seismic reflection profiles is contained in Goforth, et al. (1979). The data processing will be discussed at some length in the next section.

Fig. 11. The location of the seismic reflection profiles E-1, E-3 and N-3. The borehole control points are also plotted. The small numbers, by the profiles, refer to vibration point numbers.



YUCCA FLAT NEVADA



PROCESSING OF THE SEISMIC REFLECTION PROFILES
AND VELOCITY ANALYSIS

The three seismic reflection profiles available for analysis were VIBROSEIS^(R) data and were initially cross correlated with the source waveform to recover zero phase wavelet seismograms. The records were static corrected for elevation to a datum of 4300 ft. and first arrivals were muted. VELAN^(R) velocity scans were performed at numerous intervals on all three lines. VELAN^(R) analysis is a standard velocity scan program which computes trial normal moveout corrections and tests for coherence within certain time windows. High coherence indicates that the rms velocity (approximated by the stacking velocity) has been correctly determined and thus the velocity as a function of depth is determined. There are the critical assumptions of horizontal layering and lateral homogeneity inherent in this procedure. Departures from these assumptions result in over-estimates of the rms velocity. For homogeneous layers, dip alone will produce an over-estimate proportional to the cosine of the dip angle. Lateral heterogeneity within the limits of the geophone spread along with diffraction phenomena result in even greater errors. This is complicated by the fact that reliable velocity estimates require a large geophone spread in order to sample the large moveout on the tail of the travel time curve. Within Yucca Flat strong lateral variation due to faulting resulted in very

poor velocity estimates at depth; the shallow velocity structure, down to approximately 500 m was adequately determined. Many of the VELAN(R) profiles were unusable, and those that were used produced structural relief estimates which were inconsistent with the gravity and borehole analysis. The seismic sections were migrated by a finite difference scheme after stacking and are displayed in figures 12, 13, 14.

The lateral velocity variations result in a degraded common mid-point stack (CMP) and subsequent migration of the stack is also in error. The solution to this difficulty lies in migration of the original, unstacked data and possibly the use of migration velocity determination analogous to the normal moveout velocity (the normal moveout correction and stack is the correct migration of data observed over horizontal stratification). Several approaches to this problem have been outlined. Satlegger (1975) and Dohr and Stiller (1975) proposed migration velocity determination and Doherty and Claerbout (1976) offer a procedure for approximate migration before stack. These processes are complicated by the fact that migration calculations are relatively more costly to perform than normal moveout corrections in that the better algorithms are based on wave theory rather than geometrical ray theory. Schultz and Claerbout (1978) point out that CMP gathers and stacks are generally not realizable wave fields especially where there are significant lateral velocity variations. They propose to migrate stacks of constant ray parameter (slant stacks). In this process a number of beams would be formed and each beam migrated separately, a very costly procedure. The E-3 section was processed in

Fig. 12. This section is a migrated, common midpoint stack of the east-west seismic line E-1. The vibration points are numbered across the top. The total two-way travel time is 4 seconds.

Fig. 13. This section is a migrated, common midpoint stack of the east-west seismic line E-3. The vibration points are numbered across the top. The total two-way travel time is 4 seconds.

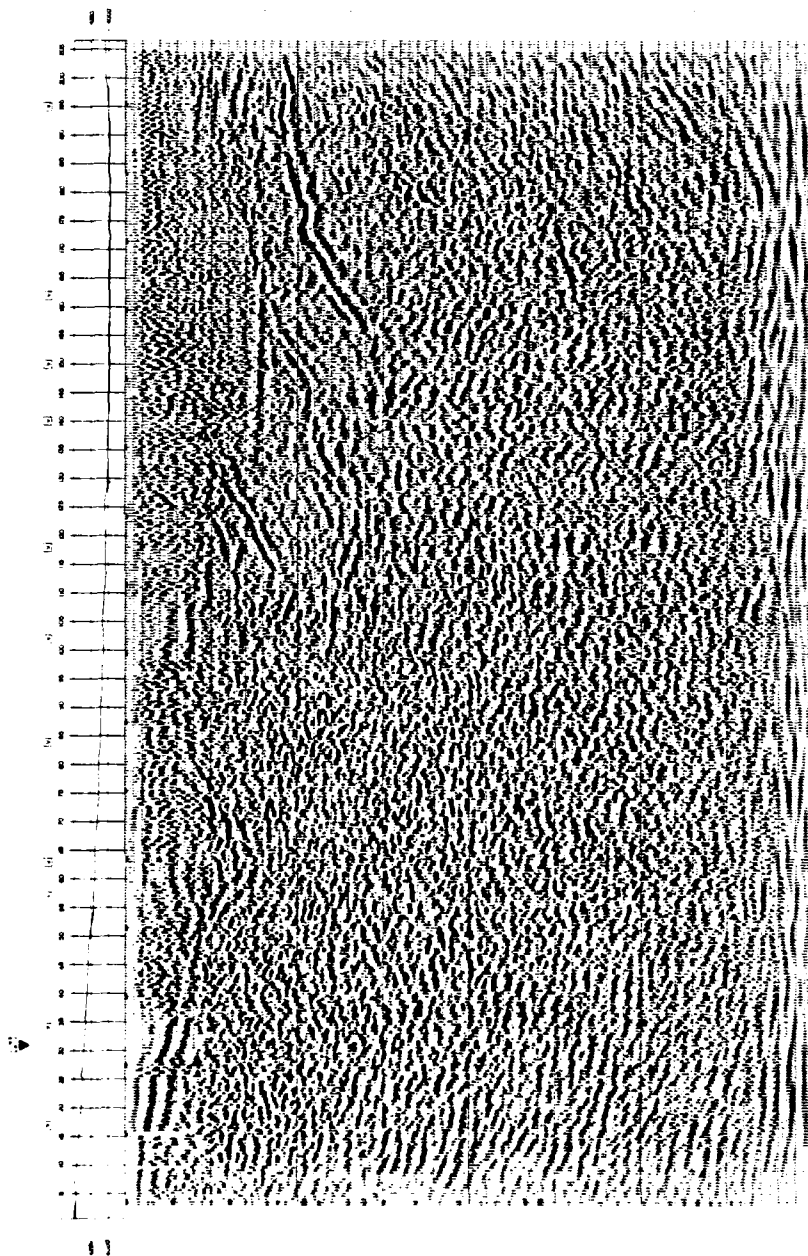


Fig. 14. This section is a migrated, common midpoint stack of the north-south seismic line N-3. The vibration points are numbered across the top. The total two-way travel time is 4 seconds.

a manner similar to the method described by Doherty and Claerbout (1976). Each normal moveout corrected CMP gather was migrated independently with a rather arbitrary choice of velocity function, a new velocity analysis was performed, and the migrated gathers were stacked with the new velocity. This processing was more expensive (24 times) than conventional processing, but not as expensive as migration of common source gathers would have been. The "migration before stack" section is shown in figure 15. The new velocity analysis improved the deeper velocity estimates by over ten percent.

The choice of a velocity function suitable for use in depth estimation was complicated by the lack of good velocity scans and the sparsity of deep velocity logs. It was not possible to construct laterally variable velocity models; however, reasonable results were obtained with a single velocity function. A comparison of interval velocity data from areas 3,4,6, and 7 is made in figure 16. The velocity function defined by borehole UE6E is close to the median and is the deepest available hole. An uphole velocity survey conducted in UE10BD by LANL and LLL agrees quite well with that in UE6E. Some holes in Area 7 and Area 3 have much lower velocities down to a 600 m depth and some Area 7 holes show rather higher velocities at shallow depth. Figure 17 is a comparison of the UE6E velocity function with the original $VELAN^{(R)}$ and "migration before stack" velocity functions. The velocity analyses chosen are the best available. They agree quite well in the shallow regions, but diverge at depth. The conventional $VELAN^{(R)}$ would produce errors of 100 m in depth. The UE6E velocity function was chosen as the

Fig. 15. Seismic reflection profile E-3. This is the same data shown in figure 13 with different processing. In this case the common midpoint gathers were migrated prior to stacking and a new stacking velocity was derived which was less effected by lateral velocity variation. The vibration points are numbered across the top. The total two-way travel time is 4 seconds.

Fig. 16. Average velocity as a function of depth determined from interval velocities at Yucca Flat, Nevada. The curve labeled UE6E is from a deep borehole located in the southern portion of the basin (see figure 11). The UE6E curve represents the median choice for the velocity function.

AVERAGE VELOCITY VS DEPTH
YUCCA FLAT, NEVADA
INTERVAL VELOCITY SURVEYS FROM
AREAS 3, 4, 6, 7 AND 10

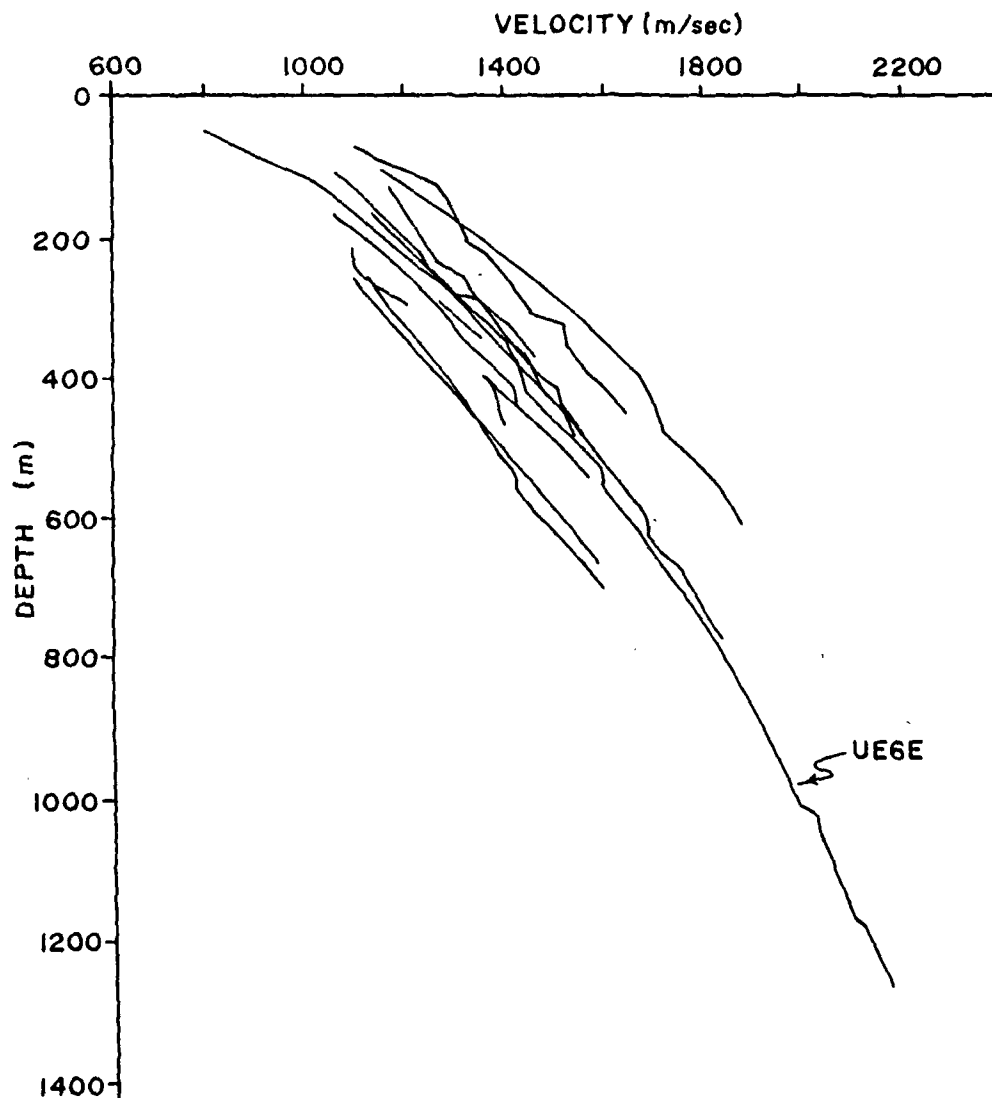
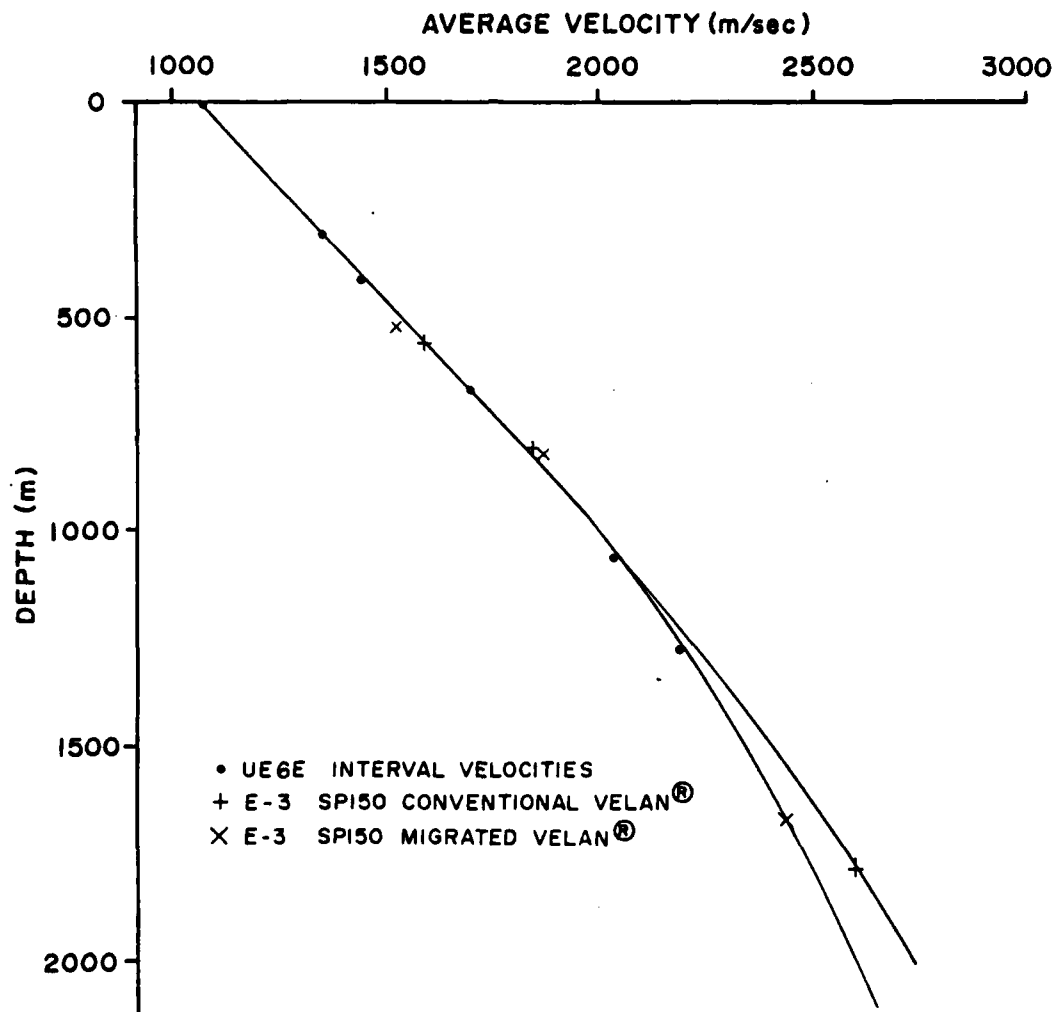


Fig. 17. The velocity functions derived from stacking velocities and the UE6E interval velocities. SP150 on profile E-3 is located only 5 kilometers from UE6E in an area of rather uniform structure. Notice that the migration before stack function is in better agreement with the UE6E function at depth and that little difference is present among the three estimates above 700 m depth.

COMPARISON OF VELOCITY FUNCTIONS YUCCA FLAT, NEVADA



standard and has been used in all depth estimates from the reflection data. This function may need modification in Areas 3 and 7 (profile E-3 is in Area 3), but it serves quite well in most of the basin.

ANALYSIS OF THE SEISMIC SECTIONS AND GRAVITY MODEL

The three seismic sections, E-1, E-3 and N-3, have been analyzed in an attempt to define the most prominent geologic features of the Yucca Flat Basin. The seismic sections have been compared to the gravity model and to the borehole data with the UE6E velocity model providing depth to time conversion.

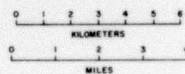
The F1B gravity model and geologic map shown in figure 18 demonstrate several important features of the basin. The deepest part of the basin is in the southeast. A saddle separates the deeper basin from a bilobate northern basin. The saddle trends northwest along the strike of several faults seen on the eastern and western margins of the valley. The western boundaries of these deeper, eastern basins will be referred to as the Carpetbag Fault system as the fault segment so named is coincident with it. The better known Yucca Fault runs down the center of the eastern basins. Both the Yucca and Carpetbag faults have right lateral strike slip component of motion as well as dip slip. A narrow horst, which rises to within a hundred meters of the surface, isolates a string of shallower smaller basins on the west from the main eastern basins.

The N-3 line unfortunately runs parallel to the western basin and slightly to the west of its center. This causes the reflections recorded to migrate from out of the plane of the section, thus pro-

Fig. 18. The three seismic profiles superimposed on a map of the Tertiary-Paleozoic interface and normal faults from the geologic maps. Notice the Yucca Fault in the middle of the basin and also the north-west trending faults in the northwest and east central portions of the map, which align with the saddle in mid-basin. The contour interval is 100 m.



YUCCA FLAT
NEVADA



viding more limited resolution of vertical depth. The N-3 section was successful in recovering structural information from below the basin and possibly a mantle reflection at 10.7 seconds two-way travel time near vibration point 140.

The two east to west trending seismic lines provide very good structural information. In order to facilitate the interpretation of these sections the F1B model was converted into time sections along the three reflection lines and then overlain on the migrated common depth point sections, as shown in figures 12, 13, and 14. Prominent reflecting events and faults delineated by diffractions were traced onto the overlays, as seen in figures 19, 20, and 21. In many areas the correlation between the gravity anomaly and the seismic reflections is quite good, but in other areas the Paleozoic contact does not appear to be a conspicuous reflector. In these cases the deeper reflections may be masked by thin, high velocity welded tuff units at shallower depths. The horst, bounded on the east by the Carpetbag Fault system, is evident, as is the Yucca Fault. Dip slip motion on these faults, especially the Carpetbag, accounts for the asymmetric basin that has recently developed at Yucca Flat. The dips of these faults seem to be somewhat low for normal faults, between 45° and 60° . Note that the curved lines drawn on the time sections (which map nonlinearly into depth) would appear as planes in a depth section. West dipping faults on the eastern end of the lines have steeper dips on the order of 70° and are conjugate to the basin forming faults. In section E-3 the water table accounts for the horizontal reflector at 0.7 seconds travel

Fig. 19. An interpretation of the first second of two-way travel time for the E-1 profile shown in figure 12. The depth scale is derived from the UE6E velocity function. The continuous, light line is from the gravity model shown in figure 8. The short, heavy lines mark the presence of coherent reflectors. Notice the agreement of the gravity model with coherent reflections between vibration points 20 to 60 and 70 to 150.

INTERPRETATION OF
LINE E-1 MIGRATED SECTION
AND GRAVITY MODEL FIB
YUCCA FLAT, NEVADA

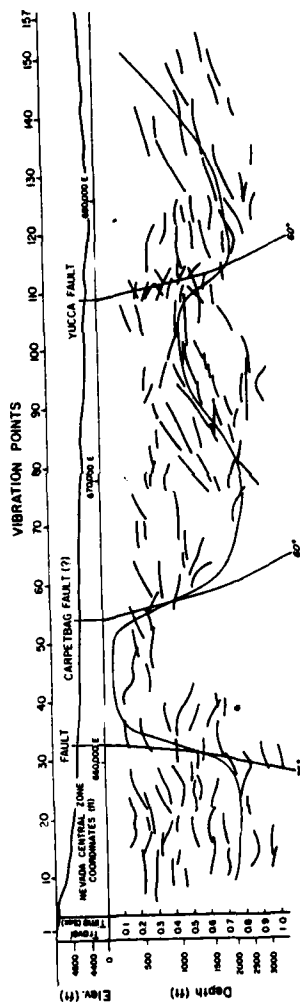


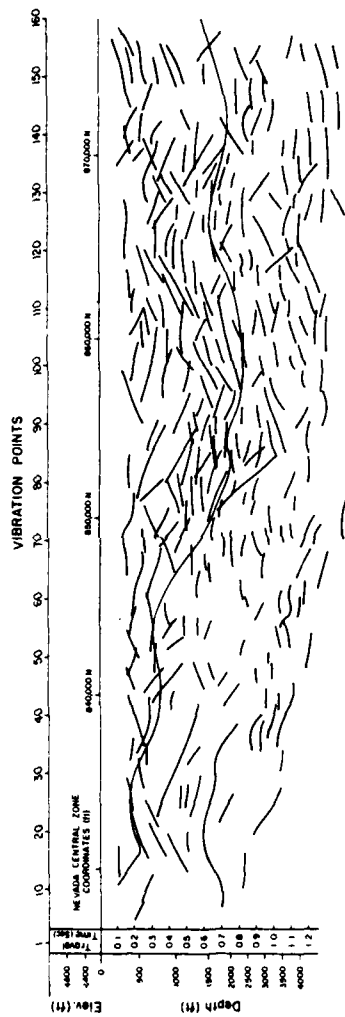
Fig. 20. An interpretation of the first 1.5 seconds of two-way travel time for the E-3 profile shown in figure 13. The depth scale is derived from the UE6E velocity function. The continuous, light line is from the gravity model shown in figure 8. The short, heavy lines mark the presence of coherent reflectors. In the interval between vibration points 130 and 160 the agreement of the gravity model with the reflectors is not high. The resolution in this area is not as high in the three-dimensional gravity model as in the two-dimensional model presented in Goforth, et. al. (1979).

This geological cross-section illustrates the subsurface structure of the Nevada Central Zone. The vertical axis on the left represents 'Depth (ft)' from 0 to 18,000, with major ticks every 2,000 feet. The horizontal axis at the top represents 'VIBRATION POINTS' from 0 to 200. The diagram shows several distinct geological features:

- Topography:** A dashed line at the surface indicates the ground profile, with peaks around vibration points 100 and 170.
- Geological Formations:**
 - Yucca Fault:** A major fault line running vertically through the center of the section, labeled 'YUCCA FAULT'.
 - San Joaquin Fault:** A fault line located to the right of the Yucca Fault, labeled 'SAN JOAQUIN FAULT'.
 - Other Faults:** Several smaller faults are indicated by dashed lines and labeled 'FAULT' at various depths and locations.
 - Stratigraphic Units:** Different rock layers are shown with various line patterns. Labels include 'sandstone' (appearing multiple times), 'shale', and 'limestone'.
- Seismicity:** A series of curved lines with arrows represent seismic wave propagation or focal mechanism solutions, showing a prominent event around vibration point 100 and depth 10,000 ft.
- Scale and Orientation:** The diagram is oriented with depth increasing downwards. The horizontal scale is in vibration points, with a total range of 200 units.

Fig. 21. An interpretation of the first 1.2 seconds of two-way travel time for the N-3 profile shown in figure 14. The depth scale is derived from the UE6E velocity function. The continuous, light line is from the gravity model shown in figure 8. The short, heavy lines mark the presence of coherent reflectors. In figure 18 it is evident that line N-3 runs parallel to and on the margin of a synform. This geometry causes the reflectors to migrate out of the plane of the profile, a difficulty which is impossible to overcome quantitatively. In spite of this problem the section shows more detail below the basin than either of the east to west profiles

INTERPRETATION OF
LINE N-3 MIGRATED SECTION
AND GRAVITY MODEL FIB
YUCCA FLAT, NEVADA



time. The volcanic units dip to the west at approximately 45° . This is due to tectonic rotation by the Carpetbag and Yucca Fault systems.

Dip slip motion on the Carpetbag Fault probably postdates the deposition of the volcanics and hence is less than about 11 million years old. The early opening of the basin at Yucca Flat is probably part of the general east-west extension of the Great Basin associated with the progressive development of the San Andreas Fault (Atwater, 1970). The strike slip motion results from a progressive reorientation of the stress field due to major plate interactions. The Yucca fault represents an eastward migration of the locus of faulting as strike slip motion and constraints, such as the Climax Stock, have become more important (Oldow, personal communication, 1981). The Yucca fault generally has less than 200 meters of displacement on it. The saddle region, which was not traversed by seismic lines in the eastern basin, is likely to be a remnant of a previous topographic high related to northwest to southeast trending faults which predate the volcanics. In the saddle the Yucca-Carpetbag Fault system breaks up into a very diffuse zone of en echelon faults known as the Topgallant system. The geometrical features observed in the Yucca Flat geophysical model now have a structural interpretation consistent with the regional tectonic trends.

The combined interpretation of geologic, gravity and seismic data depicts the general structural configuration of the basin very well. Major normal faults on the west rotate the basin down about a broad hinge zone at the eastern margin. This structural development occurred after deposition of the volcanics. A pre-existing northwest structural lineation forms a saddle which divides the basin into north and south parts. This saddle affects later structural elements such as the Carpetbag and Yucca Fault systems in the central saddle region. A tectonic pattern of increasing strike slip motion on the western bounding faults in recent time can explain the shift of activity from the Carpetbag to the Yucca Fault systems.

Body wave magnitude variations, when properly normalized to constant explosion yield, show a variation which correlates with the model presented here. In particular, location of the explosions relative to the Carpetbag fault and to the saddle is highly significant. The theoretical response of this structure will be calculated to further verify this hypothesis and provide a predictive capability.

REFERENCES

- Atwater, T., Implications of plate tectonics for the Cenozoic tectonic evolution of western North America, *Geol. Soc. Am. Bull.*, 81, pp. 3513-3535, 1970.
- Burkhard, N. and D.D. Jackson, Application of stabilized linear inverse theory to gravity data, *J. Geophys. Res.*, 81, pp. 1513-1518, 1976.
- Cordell, L., Sedimentary facies and gravity anomaly across master faults of the Rio Grande rift in New Mexico, *Geology*, 7, pp. 201-205, 1979.
- Cordell, L. and R.B. Henderson, Iterative three-dimensional solution of gravity anomaly data using a digital computer, *Geophys.*, 33, pp. 596-601, 1968.
- Doherty, S.M. and J.F. Claerbout, Structure independent velocity estimation, *Geophys.*, 41, pp. 850-881, 1976.
- Dohr, G.P. and P.K. Stiller, Migration velocity determination: Part II. Applications, *Geophys.*, 40, pp. 6-16, 1975.
- Dorman, L.M. and B.T.R. Lewis, The use of nonlinear functional expansions in calculation of the terrain effect in airborne and marine gravimetry and gradiometry, *Geophys.*, 39, pp. 33-38, 1974.
- Eaton, G.P., R.R. Wahl, H.J. Prostka, D.R. Mabey and M.D. Kleinkopf, Regional gravity and tectonic patterns: Their relation to late Cenozoic epeirogeny and lateral spreading in the western Cordillera, in Smith, R.B. and G.P. Eaton, eds., Cenozoic Tectonics and Regional Geophysics of the Western Cordillera, *Geol. Soc. Am. Mem.* 152, pp. 51-91, 1978.
- Eckel, E.B., ed., Nevada Test Site, *Geol. Soc. Am. mem.* 110, 1968.
- Felch, R.N., A Three-Dimensional Gravity Model of Basin Structure, Yucca Flat, Nevada, M.S. Thesis, Texas Christian University, 1979.
- Goforth, T., J. Ferguson and E. Herrin, Crustal Studies of the Nevada Test Site: Interpretation of S.M.U. line E-3, Final Technical Report to the Air Force Office of Scientific Research, Contract Number: F49620-77-C-0216, Southern Methodist University, 1979.

- Gunn, P.J., Linear transformations of gravity and magnetic fields, *Geophys. Prosp.*, 23, pp. 300-312, 1975.
- Hazelwood, R.M., D.L. Healey and C.M. Miller, U.S. Geological Survey Investigations of Yucca Flat, Nevada Test Site Part B - Geophysical Investigations, Tech. Letter. NTS-45, 1963.
- Healey, D.L., Gravity and seismic study of Yucca Flat, Nevada Test Site, Nye County, Nevada, in *Mining Geophysics Vol. I*, Society of Exploration Geophysics, 1966.
- Healey, D.L., Application of gravity data to geologic problems at Nevada Test Site, in Eckel, E.B., ed., *Nevada Test Site*, Geol. Soc. Am. Mem. 110, 1968.
- Nelder, J.A. and R. Mead, A simplex method for function minimization, *Comp. J.* 7, pp. 308-313, 1965.
- Oldenburg, D.W., The inversion and interpretation of gravity anomalies, *Geophys.*, 39, pp. 526-536, 1974.
- O'Neil, R., Function minimization using a simplex procedure, *Appl. Stat.*, 20, pp. 338-345, 1971.
- Parker, R.L., The rapid calculation of potential anomalies, *Geophys. J. Roy. Astr. Soc.*, 41, pp. 447-455, 1972.
- Parker, R.L. and S.P. Huestis, The inversion of magnetic anomalies in the presence of topography, *J. Geophys. Res.*, 79, pp. 1587-1593, 1974.
- Peters, L.J., The direct approach to magnetic interpretation and its practical application, *Geophys.*, 18, pp. 290-320, 1949.
- Satlegger, J.W., Migration velocity determination: Part I. Philosophy, *Geophys.*, 40, pp. 1-5, 1975.
- Schultz, P.S. and J.F. Claerbout, Velocity estimation and downward continuation by wavefront synthesis, *Geophys.*, 43, pp. 691-714, 1978.
- Shepard, D., A two-dimensional interpolation function for computer mapping of irregularly spaced data, *Geography and Properties of surfaces series*, n 15, Harvard University, 1968.
- Smith, R.A., A uniqueness theorem concerning gravity fields, *Proc. Comb. Phil. Soc.*, 57, pp. 865-870, 1961.
- Tikhonov, A.N., Solution of incorrectly formulated problems and the regularization method, *Soviet Math. Dok.*, 4, pp. 1035-1038, 1963.

Tikhonov, A.N., V.B. Glasko, O.K. Litvinenko and V.P. Melikhov, Analytic continuation of a potential in the direction of disturbing masses by the regularization method, *Izv. Earth Phys.*, 12, pp. 30-48, 1968.

Tsirul'skiy, A.V., The reduction of observed potential fields to a single level, *Izv. Earth Phys.*, 3, pp. 85-89, 1968.

Tsirul'skiy, A.V. and L. Ya. Ospishcheva, An algorithm for the reduction of observed potential field values to a common level, *Izv. Earth Phys.*, 4, pp. 105-111, 1968.